TABLE OF CONTENTS

		Page	
NOMENCLATURE		v	1/A7
I.	INTRODUCTION	1	1/A9
II.	EXPERIMENTAL APPARATUS	5	1/A13
	A. Low Pressure Stress-Strain Apparatus: 0.7 GPa B. Constant Pressure Stress-Strain Apparatus 1.1 GPa		
III.	EXPERIMENTAL LUBRICANTS	9	1/B3
IV.	EXPERIMENTAL RESULTS	10	1/B4
	A. Liquid Lubricants B. Solid Polymers		
V.	APPLICATION OF THE MODEL TO EHD TRACTION PREDICTIONS	14	1/B8
VI.	APPLICATION OF THE MODEL TO EHD FILM THICKNESS PREDICTION	18	1/B12
	A. Shear Rheological Model B. Derivation of the Governing Equations C. Method of Solution D. Physical Input Data E. Results F. Discussion G. Conclusions		
REFERENCES		41	1/D7
APPENDICES			
A.	DESCRIPTION OF EXPERIMENTAL FLUIDS	43	1/D9
B.	DERIVATION OF PRESSURE GRADIENT EQUATIONS	47	1/D13

NASA Contractor Report 3272

Surface Temperatures and Glassy State Investigations in Tribology - Part III

Scott S. Bair and Ward O. Winer

GRANT NSG-3106
APRIL 1980

NASA

NASA Contractor Report 3272

Surface Temperatures and Glassy State Investigations in Tribology - Part III

Scott S. Bair and Ward O. Winer
Georgia Institute of Technology
Atlanta, Georgia

Prepared for
Lewis Research Center
under Grant NSG-3106

National Aeronautics
and Space Administration

**Scientific and Technical
Information Office**

1980

Blank Page

TABLE OF CONTENTS

Page

NOMENCLATURE v

I. INTRODUCTION 1

II. EXPERIMENTAL APPARATUS 5

A. Low Pressure Stress-Strain Apparatus: 0.7 GPa
B. Constant Pressure Stress-Strain Apparatus 1.1 GPa

III. EXPERIMENTAL LUBRICANTS 9

IV. EXPERIMENTAL RESULTS 10

A. Liquid Lubricants
B. Solid Polymers

V. APPLICATION OF THE MODEL TO EHD TRACTION PREDICTIONS . 14

VI. APPLICATION OF THE MODEL TO EHD FILM THICKNESS PREDICTION 18

A. Shear Rheological Model
B. Derivation of the Governing Equations
C. Method of Solution
D. Physical Input Data
E. Results
F. Discussion
G. Conclusions

REFERENCES 41

APPENDICES

A. DESCRIPTION OF EXPERIMENTAL FLUIDS 43

B. DERIVATION OF PRESSURE GRADIENT EQUATIONS 47

Blank Page

NOMENCLATURE

a = Hertzian contact radius

$E_{1,2}$ = Modulus of elasticity of the contact materials 1 and 2 respectively

E_r = Equivalent modulus of elasticity of the contact materials, where, $E_r^{-1} = \frac{1}{\pi}\left(\frac{1-\sigma_1^2}{E_1} + \frac{1-\sigma_2^2}{E_2}\right)$

G = Material parameter, where $G = (\alpha E)$ dimensionless

G_∞ = Elastic shear modulus of the lubricant

h = film thickness

h_o = nominal film thickness

H = film thickness parameter, where $H = h/R$, dimensionless

H_o = nominal film thickness parameter, where $H_o = h_o/R$, dimensionles

L = Length of the contacting cylinders

m = slope of the limiting shear stress-pressure relation

p = pressure

p' = pressure gradient, $p' = \frac{dp}{dx_1}$,

Q = volumetric flow rate

r = radius of the contacting cylinders

R = equivalent radius of the contacting cylinders where $1/R = 1/r_1 \pm 1/r_2$

t = time

u_{11} = lower surface velocity in x_1 direction

u_{21} = upper surface velocity in x_1 direction

u = rolling speed, where $u = u_{11} + u_{21}$

U = speed parameter where $U = \left(\frac{\mu_o U}{ER}\right)$, dimensionless

w = load

w/L = load per unit length

W = load parameter, where $W = \left(\frac{E \cdot R}{w/L}\right)$, dimensionless

x_1 = horizontal coordinate axis (origin is at the center of the Hertzian contact)

x_3 = vertical coordinate axis

α = pressure coefficient of viscosity

μ = viscosity

μ_o = zero pressure value of viscosity

$\sigma_{1,2}$ = Poisson's ratio for contact materials 1 and 2 respectively

τ_L = limiting shear stress

τ_1 = lower surface shear stress

τ_2 = upper surface shear stress

τ_{L_o} = zero pressure value of limiting shear stress

Σ = slide/roll ratio, where $\Sigma = 2\,\frac{u_{21} - u_{11}}{u_{21} + u_{11}}$

$\hat{\tau}_i = \frac{\tau_i}{\tau_L}$, i = 1 or 2

$\hat{t} = \frac{\mu}{\tau_L G_\infty}\,\frac{d\tau}{dt}$

$\hat{\dot{\gamma}} = \frac{\mu}{\tau_L}\,\dot{\gamma}$

I. INTRODUCTION

In a previous report [1] the authors have shown that under well defined conditions many liquid lubricants behave as non-equilibrium amorphous solids in the Hertzian region of elastohydrodynamic contacts. They have also presented a simple shear rheological constitutive equation [2] which requires only three material properties as functions of pressure and temperature. These are the low shear stress viscosity ($\mu_o(p,T)$), the limiting elastic shear modulus ($G_\infty(p,T)$), and the limiting shear stress ($\tau_L(p,T)$).

The low shear stress viscosity of many lubricants has been reported in the literature for nearly a century and is therefore a familiar concept. The limiting elastic shear modulus (or high frequency shear modulus) is less familiar in the lubrication literature but nevertheless has been measured for many years by several techniques including ultrasonics [3]. The limiting shear stress of liquid lubricants has been the subject of speculation for many years [4] and indeed the nature of traction measurements in EHD contacts has led several researchers to support that view for sometime [5,6,7,8].

The first measurements of limiting shear in liquid lubricants, independent of EHD-type experiments, were reported by Bair and Winer [9] at temperatures and pressures typical of the Hertzian region of EHD contacts. Because at those temperature-pressure conditions the material was in the amorphous solid state, some if not all of its properties could be expected to be a function of the history (state path) to which the material was subjected as it went from the liquid to the amorphous solid state [10]. Qualitatively, where the material passes through the

liquid-solid transition will be one of the defining characteristics of the material in the amorphous state [10]. The higher the pressure at which the transition occurs, the higher will be the density and limiting shear stress in the amorphous state.

In the previously reported limiting shear stress research [2] the material had been subjected to an isobaric cooling process for reasons of convenience in the experimental technique. However, in a typical EHD contact at low slide-roll ratio the temperature rise is small [11] and the process the lubricant is subjected to as it passes through the contact is closer to isothermal compression. Therefore, for the same temperature and pressure, the material in the limiting shear stress experiment had passed through the liquid-solid transition at a higher pressure (therefore higher density in the amorphous solid) than would occur in the EHD contact. This might be expected to cause the measured limiting shear stress to be higher (at least different) than would be the case in the EHD contact at the same temperature and pressure. This may also explain why the predicted traction-slide-roll ratio curves [2] based on the laboratory limiting shear stress measurements had a maximum about ten percent higher than the EHD measured values even though the increasing portion of the curves agree quite well. One of the objectives of this research was to examine the effect of history on the limiting shear stress of liquid lubricants. It will be shown that the isothermal compression history results in a lower limiting shear stress and one which agrees with the peak traction measurement in EHD contacts.

The shear stress-strain behavior, including limiting shear stress, of solid lubricating plastic materials have also been measured under pressure. The history of the solid plastic lubricating materials in a lubricated contact would not be expected to be important in determining the shear properties of the lubricant because they do not experience a liquid-solid transition in the contact. However, the previous processing history of the material, when it may have passed between liquid and solid states, will influence the properties. The previous processing history is known to influence the yield stress of solid polymers [12].

The shear rheological model with measured limiting shear stress was also used to predict EHD traction slip roll ratio behavior. Those predictions were compared with EHD data published by Johnson and Tevaarwerk and measured in our laboratory. Side slip and spin were introduced into the model. Side slip due to misalignment was shown to be very influential on traction both in the model and the measurements.

A Grubin-like EHD inlet analysis utilizing a non-linear viscous fluid model with a limiting shear stress is also reported. The shear rheological equation requires only a low shear stress viscosity and the limiting shear stress both functions of pressure. Values employed for these properties are taken from measurements on typical lubricants. Reductions of EHD film thickness are found to be up to 40 percent compared with the standard Grubin prediction for typical operating conditions. Slide-roll ratio, limiting shear stress dependence on pressure, and atmospheric pressure value of limiting shear stress are

new variables required to determine film thickness with the first two being more important than the last. The EHD film thickness is reduced by increasing slide-roll ratio and/or decreasing the pressure dependence of the limiting shear stress.

II. EXPERIMENTAL APPARATUS

Two apparatus were used to measure the high-pressure shear rheological response of lubricants to 1.1 GPa (162,000 psi). One, the low pressure stress-strain apparatus was used in some of the isobarically cooled investigations and the other, referred to as the constant pressure stress-strain apparatus, was used in all of the isothermal compression experiments and all of the experiments involving solid polymers.

A. Low Pressure Stress-Strain Apparatus: 0.7 GPa

As reported previously [2], an apparatus was constructed to measure the mechanical shear properties of glassy lubricant samples to pressures of 0.7 GPa. It is shown schematically in Figure 1. The glassy sample is formed in an annular groove by cooling at elevated pressure. The groove is kept filled by a sample reservior which is sealed from the working fluid (gasoline) by an isolator piston. The sample material can be sheared in the annulus by the development of a pressure difference across the driving piston. The shear stress is determined by knowing the geometry and measuring the differential pressure by two pressure transducers. The sample strain is determined by the displacement of the driving piston measured with an LVDT. This signal can also be used to measure the strain rate. The shear stress (pressure difference), the strain (piston displacement) and time are recorded on an x-y-y recorder. Sample temperature is determined by a thermocouple imbedded in the pressure vessel wall.

At moderate working temperatures such as those for 5P4E (-20 to 35C),

and elevated pressures, the seal friction is negligible and no shearing force across the piston can be maintained when the test material is above its glass transition temperature. However, with N1* the temperature required to go into the glassy region at moderate pressures is so low (-40C) that a correction for seal friction must be employed. The seal friction at low temperature was calibrated by using gasoline as the test fluid which has very low viscosity at the test temperature and pressure. Therefore, at the low shearing rate of the experiment, the driving force on the piston was assumed to be due to seal friction. This seal friction was typically less than five percent of the maximum shear stress measured for N1.

Referring to Figure 1 the sequence of a typical experiment is the following: with the sample in the apparatus, the system is heated to a temperature high enough to keep the sample in the liquid region at the predetermined pressure to be used. The system is then brought up to pressure with the valve open insuring uniform pressure throughout the apparatus. The system is then cooled to the desired temperature at or below the dilatometric liquid-solid transition while maintaining constant pressure. The isolating piston movement accommodates sample volume change during these state changes. The valve is then closed isolating the regions above and below the driving piston. Stress is applied to the sample by either increasing or decreasing the pressure on the bottom of the driving piston by varying the supply pressure. The pressure difference is measured by the two pressure transducers.

*The fluids are described in the Appendix.

The driving piston displacement and velocity are measured by the LVDT. By the nature of the device, when the piston moves downward the pressure level decreases and when it moves upward the pressure level increases. The pressure level changes can be kept to a minimum by keeping the strain (piston displacement) small for a given measurement.

B. Constant Pressure Stress-Strain Apparatus 1.1 GPa

Previous shear strength measurements [1,2] were made in this laboratory with an apparatus which derived the force necessary to shear the sample from the pressure of the pressurizing medium. Consequently, as the sample was strained the hydrostatic pressure changed. A new apparatus, Figure 2, has been constructed to perform at a nearly constant pressure, extend the pressure range to 1.1 GPa (162 kpsi), and accommodate large changes in volume of liquid samples. In addition, a replacement cell for the testing of solid polymer samples has been provided.

The apparatus includes an integral pressure intensifier whose high pressure piston forms one of the closures of a translating cylindrical pressure vessel. The other closure is a fixed piston. The vessel can be driven hydraulically by oil supplied to either end of the vessel. For solid polymers the experimental cell enclosed in the vessel is simply a fixture for holding and shearing an annulus shaped sample. For liquid samples, the cell includes a reservoir with an isolating piston to replenish the sample in the annulus as its volume is reduced on pressurization.

The vessel can be moved a small distance before the cell contacts the fixed piston allowing calibration of the closure seal

friction. Further movement of the vessel produces a relative motion between the cell and the vessel, straining the sample. The vessel displacement, hence sample strain, is measured by an LVDT transducer. The hydraulic pressure which drives the vessel is measured by a commercial pressure transducer. The strain rate is controlled by regulating the hydraulic oil flow rate. Temperature is determined with a copper-constantan thermocouple in the wall of the vessel. The apparatus is submerged in an oil bath for temperature control.

The pressure of the large end of the intensifier is measured with a precision Heise bourdon tube gauge and the pressure of the medium in the vessel (diester) is determined from the known intensifier area ratio and measured seal friction. Hydraulic pressure acting on the vessel (sample stress) and vessel displacement (sample strain) are recorded as functions of time on a two function x-y-y plotter.

III. EXPERIMENTAL LUBRICANTS

The materials included in this study were

Liquids	Solids
5P4E	Teflon
N1	Polyvinylchloride
N1 + Polymer	Acrylic (extruded)
MCS 460	Nylon
KRYTOX	
Santotrac 50	
XRM 177F	
LVI 260	
Vitrea 79*	

Description of liquids may be found in Appendix A. Solid polymers were obtained form a local plastic supply house in rod form and machined to fit the apparatus.

*Samples received from K. L. Johnson, Cambridge University.

IV. EXPERIMENTAL RESULTS

The data take the form of stress versus strain curves obtained from an x-y plotter along with a plot of time versus strain from which strain rate is determined. Experiments involving isobaric cooling history were begun at atmospheric pressure above the glass transition temperature as determined by dilatometry, pressurized at that temperature, then cooled to the test temperature. To determine limiting shear stress (τ_L) each sample was sheared plastically at various strain rates. Figure 3 is a typical plot of shear stress versus shear strain-rate for the lubricant N1. At the lowest pressure, viscous behavior is exhibited at the lower strain rates by the slope of the curve tending toward 45 degrees. The viscosity of the sample must be at least 10^9 Pas at temperature and pressure in order to measure limiting shear stress due to the limited shear strain rate provided by this instrument.

A. Liquid Lubricants

1. Limiting Shear Stress

As a continuation of previous work [2], limiting shear stress was measured for Krytox (perfluorinated polyether) and N1 plus four percent PAMA (polyalkylmetacrylate) at one pressure and MCS 460 (synthetic hydrocarbon) at two pressures, (Figure 4). N1 (naphthenic base oil) is also shown for comparison. The history is isobaric cooling. A small reduction in τ_L results from the addition of polymer to N1, consequently some loss in EHD traction would be expected.

Since it is known [10] that the history of an amorphous material as it goes from the liquid to the solid state influences the resulting

density of the amorphous solid, an experiment was performed with 5P4E to determine the effect of history on limiting shear stress. The upper curve in Figure 5 represents the limiting shear stress versus pressure at 38C resulting from isobaric cooling in the constant pressure shear stress apparatus. Included are data points from the low pressure apparatus and high stress viscometer previously reported [2]. The curve below represents data for the same material and temperature subjected to isothermal compression. The compression history produces a lower τ_L than the cooling history as would be expected since the density is also lower for the compressional history. Also in Figure 5 is the liniting shear stress for 5P4E at 80C for compressional history. Since isothermal compression is the history most representative of the inlet of an EHD zone where a solid transition may occur, all succeeding data will be for that history.

In Figure 6, pressure-limiting shear stress isotherms are plotted for N1 (naphthenic base oil), Krytox (perfluorinated polyether), Santotrac 50 (cycloaliphatic hydrocarbon traction fluid), and the samples of K. L. Johnson, Vitrea 79 and LVI 260. An attempt was made to measure the stress-strain behavior of XRM 177F to 1.1 GPa at 22C, but no measurable shear stress was developed at the available shear rate because of its low viscosity ($< 10^2$ Pas) at that pressure and temperature. It is noteworthy that the order of the magnitude of τ_L for Santotrac 50, N1, and Vitrea 79 is the same order in which one would expect to rank them for traction coefficient.

2. Shear Modulus

The slope of the initial linear portion of the shear stress-shear strain curve yields the elastic shear modulus of the lubricant sample when corrected for the deflection of the instrument parts during the experiment. The instrument deflection was calibrated by replacing the sample cell by the solid steel slug. Figure 7 shows the shear modulus, G, of N1 versus shear rate at four pressures. At 0.91 GPa pressure the shear modulus is independent of strain rate for the range of rates shown. It is expected that at the lower pressures a limiting shear modulus, G_∞, would also be reached if the strain rate were high enough or the temperature low enough.

B. Solid Polymers

The shear rheology of polyvinyl chloride, Teflon, acrylic, and nylon are shown in Figure 8-11. Due to the volume contraction of the sample under pressure some clearance occurs between the polymer sample and the holding fixture which prevents an accurate determination of shear strain. Therefore, the abscissa of Figures 8-11 is relative deflection of the cell components. This deflection is proportional to sample strain in such a ratio that 1 mm deflection is a strain of approximately 120 percent. The area used in the shear stress calculation is the area of the sample at atmospheric pressure. The rate of deflection for the solid polymer measurements was approximately constant at 0.2 mm/s which is a strain rate of approximately 0.24 s^{-1}.

Since the viscosity of the polymer samples must be very high, the visco-plastic relaxation time [2]

$$t_{p_\ell} = \frac{\mu}{\tau_L}$$

must be long enough to produce the limiting shear stress at the rate encountered in these experiments. The ultimate or limiting shear stress for PVC and Teflon is plotted in Figure 12 along with the limiting stress of N1 and Santotrac 50. Not only are the magnitudes comparable but the slopes, $-\lambda \left.\frac{d\tau_L}{dp}\right|_T$ are approximately the same.

V. APPLICATION OF THE MODEL TO EHD TRACTION PREDICTIONS

The above mentioned isothermal compression limiting shear stress and limiting elastic shear modulus were utilized in the constitutive equation developed in the previous report [2] along with the low rate viscosity $\mu_o(P,T)$ to predict EHD traction. The contact was divided nonuniformly into a grid of 20 segments on a cord in the direction of motion and 20 such strips across the contact perpendicular to the direction of motion to permit pressure and material property variation in the contact. The following assumptions were employed; the film thickness and material temperatures were assumed uniform throughout the contact, the pressure distribution was Hertzian, the viscosity was an exponential function of pressure, the elastic shear modulus was proportional to pressure, the elastic surface compliance was proportional to the contact traction as developed by Kalker [13] and reported in Johnson and Roberts [6], and inlet zone effects were neglected. Several of these assumptions can be called into question and should be refined in subsequent development particularly those concerned with the temperature distribution and the inlet zone influence.

Although we know the film temperature is not constant the analysis is done for slide-roll ratios of less than one tenth. From other work in this laboratory under conditions similar to those used in this analysis we know the maximum surface temperature rise is usually less than 5C above the bulk temperature in this range of operating conditions. Although we have not measured lubricant temperatures at these low slide-roll ratios, work in sliding contacts would indicate they are probably less than 5 to 10C above the surface temperature.

With the above assumptions a program was written to calculate the local shear stress at each point in the grid by using a Bisection Method on the model equation with starting shear stresses of zero and 0.999 τ_L. If the Bisection Method does not find a solution as the trial shear stress reaches 0.999 τ_L, the solution is assumed to be τ_L. To obtain the time derivative term, upstream grid positions plus a convective derivative are employed for a given grid point. The average shear stress in the contact is obtained by integration over the area and the traction coefficient is the ratio of the average shear stress divided by the average pressure.

Figure 13 shows the three predicted traction curves for 5P4E, LVI 260, and Vitrea 79 at an average Hertzian pressure of 0.67 GPa and the indicated temperatures assuming that no spin or side-slip was present. For comparison the experimental data reported by Johnson and Tevaarwerk [8] are included. The prediction of peak traction seems to be in good agreement with experiment, however, the low slide-roll ratio portionof the predicted curves lie at about one third the slide-roll ratio of the experimental points.

In order to reconcile the difference at low slide-roll ratio of the predicted curves and experiment both side-slip and spin were added to the traction program. They can be added easily as two-dimensional strain to the visco-plastic or elastic plastic equations [2], but a full visco-elastic-plastic solution for spin and slip has not been completed. If, however, the viscosity is very large, then the viscous portion of the solution may be omitted by setting μ_o very large without

altering the predicted traction curve. In the same manner, if the viscosity is small, then elasticity may be omitted. The spin and side slip were considered because they may have been present in the experiment as a result of small misalignment and will be present to some extent in most EHD applications.

In Figure 14 side slip has been added to the predictions for 5P4E at two pressures. When comparing these predictions with the Johnson and Tevaarwerk data [8] a side slip angle (as defined by the illustration) of only 0.6 milli-radian was required to bring the low slide-roll ratio portion of the model into agreement with experiment as shown in Figure 15. It was assumed that no spin was present. A small amount of spin or combination of slip and spin would have the same effect. Such a small angular misalignment of machine elements is not improbable in even the most carefully assembled EHD simulators.

To further evaluate the effect of small side slip resulting from axis misalignment our ball on flat EHD simulator was modified. The modifications considered of an ability to adjust the sapphire mount to permit movement of the sapphire axis of rotation relative to the ball axis of rotation. Although precise alignment could not be determined, the relative angle could be varied by hundreds of a radian. The angle of interest is that formed between two lines in the plane of the sapphire surface both passing through the hertz contact, one parallel to the ball axis of rotation and one through the point where the sapphire axis of rotation passes through the surface. Precise alignment occurs when the sapphire axis intersects the ball axis of rotation. An

additional modification was the ability to continuously record surface velocities and traction. These signals were digitized and analyzed with a program to determine the traction-slide/roll ratio curves while the surface velocities were driven in such a manner as to sweep the slide roll ratio from negative to positive.

Figure 16 shows the traction coefficient versus slide-roll ratio relation for the mineral oil N1 at the conditions indicated and several side slip angles as predicted by the model, Figure 17 contains traction curves measured for N1 and the same conditions and four relative side slip angles. By comparing the predicted (Figure 16) and measured (Figure 17) we conclude the zero relative side slip in the measured data could be 0.015 radians. The predicted values from the model for the same measured relative side slip are shown in Figure 18. The agreement between measured and predicted values is quite good which lends credability to the rheological model and the limiting shear stress concept.

Figure 19 shows a measured traction curve for Santotrac 50. The side slip and spin were minimized within the present limitations of the apparatus. The full model prediction was not calculated but the maximum traction coefficient is in agreement with the limiting shear stress property measurement for this lubricant.

These traction measurement comparisons with the model point to the validity of the limiting shear stress model and the concept of the limiting shear stress as an important material property for determining traction in thin film lubrication.

VI. APPLICATION OF THE MODEL TO EHD FILM THICKNESS PREDICTION

The shear rheological model with a limiting shear stress used in the previous section to determine contact traction has also been used in a Grubin-type EHD film thickness analysis. This analysis was conducted by Mr. B. Gecim as his M.S. (M.E.) thesis research [14].

The study of the mechanics of elastohydrodynamic (EHD) contacts is primarily concerned with the film thickness developed and the traction force between the two surfaces. It is well accepted that these two aspects of the contact are, in a sense, separate phenomena in that the film thickness is determined by flow in the inlet region and the traction is determined by phenomena in the Hertzian region of the contact. The film thickness generation, and lubricant behavior relevant to it, has been better understood than the traction behavior.

In our previous report [2] we have proposed a visco-elastic-plastic flow shear rheological constitutive equation for the lubricant based on primary laboratory property measurements which appears to predict traction behavior in EHD contacts. In that model the lubricant reaches a limiting shear stress value as a result of a visco-plastic or elastic-plastic transition that is related to the glass transition under pressure. We have also shown this kind of behavior to occur in several lubricants. The possibility is raised of the limiting shear stress behavior influencing EHD film thickness generation if the transition were to occur in the inlet zone of the contact. The objective of this study was to examine that possibility.

The visco-plastic portion of the constitutive equation was modified and coupled with the equations of motion and conservation of mass and

used in a Grubin-type EHD inlet analysis. Isothermal, steady, incompressible conditions with negligible body and inertial forces are considered. The Grubin-type film thickness analysis is performed for an EHD line contact configuration in the fully-flooded full-film regime. The objective of this study was to determine the effect of lubricant limiting shear stress on the nominal film thickness.

Two new parameters are introduced into a classical Grubin-type film thickness analysis; sliding speed and lubricant limiting shear stress. The limiting shear stress is expressed as a linear function of pressure, at a constant temperature. In an EHD contact inlet, pressure increases by orders of magnitude, hence the limiting shear stress may also increase greatly. Therefore, only under the severe operating conditions of high sliding speeds or pressure gradients, does shear stress reach the limiting value. Under such circumstances a decrease of up to forty percent from Grubin's prediction of nominal film thickness was found.

Although the confirmation of the existence of a limiting shear stress is relatively new in the field of tribology, it is an intrinsic material property of the lubricants. Therefore it is reasonable to conclude that, under usual operating conditions, with most conventional lubricants, no drastic changes or sudden collapse in film thickness is expected. Hence the small (< 40 percent) reduction in film thickness predicted in this analysis is reasonable.

In this analysis slip between the lubricant and the boundary was not permitted. The usual no-slip boundary conditions of viscous fluid

mechanics was employed. An alternate approach to this problem has been suggested by Wilson to employ the solution technique used by Aggarwal and Wilson [15] in metal die drawing operations with a lubricant model exhibiting a limiting shear stress. That method was also employed and is reported as part of reference [14]. As discussed in [14] we believe the Aggarwal and Wilson [15] model fails to satisfy the physical constraint of conservation of mass when the limiting shear stress is reached at either surface.

Bell [16], proposed an analytical solution model for film thickness between contacting cylinders, with the Ree-Eying constitutive equation which also has a shear thinning behavior but no limiting shear stress. The analysis aimed to explain the phenomena in the case of high rolling speeds, and high viscosity where Grubin's prediction fail to match the experimental observations. However, the analysis, being restricted to the pure rolling case, lost the generality in comparison with the real contact phenomena, whereas the present study analyzes the sliding as one of the major causes of film thickness reduction. Bell's analysis suffered from the lack of data on the Ree-Eyring parameters whereas the present study does have the experimentally determined lubricant parameters (i.e., limiting shear stress parameters) to put in the analysis.

In a similar analysis to Bell's earlier work, Bell and Kannel [17] analyzed a generalized pressure dependency of viscosity, non-Newtonian Rheology of Ree-Eyring form and a time delay in pressure effect on viscosity. The time delay approach was found to provide the best

correlation with experimental measurements. However, this analysis required to specify an inlet pressure which is not a well defined parameter in the field.

A. Shear Rheological Model

The lubricant shear rheological model employed is a slightly modified version of the limiting shear stress model put forth by Bair and Winer [2] based on primary measurements. Their equation was

$$\frac{\partial u}{\partial x} = \dot{\gamma} = \frac{1}{G_\infty}\frac{d\tau}{dt} - \frac{\tau_L}{\mu}\,\ell n\left(1 - \frac{\tau}{\tau_L}\right)$$

which can be viewed as a modified Maxwell viscoelastic model with a non-linear viscous term exhibiting a limiting shear stress, τ_L. The viscous term in that model suffers from the obvious lack of symmetry about zero shear stress and is unsuitable for incorporating in an analysis. To correct this difficulty it is proposed to replace the natural logarithm with the inverse hyperbolic tangent which has essentially the same behavior in the positive shear stress range and has the advantage of having the necessary symmetry. Therefore, the modified Maxwell model becomes in dimensionless form

$$\hat{\dot{\gamma}} = \hat{\dot{\tau}} + \tanh^{-1}(\hat{\tau}) \qquad (1)$$

or in dimensional form Equation (1) becomes,

$$\dot{\gamma} = \frac{1}{G_\infty}\frac{d\tau}{dt} + \frac{\tau_L}{\mu}\tanh^{-1}\left(\frac{\tau}{\tau_L}\right) \qquad (2)$$

From Equation (2) it is seen that the three primary physical properties required to use the model are low shear stress viscosity

μ, the limiting elastic shear modulus G_∞, and the limiting shear stress τ_L, all as functions of pressure and temperature.

For very large values of the limiting shear stress (small values of $\frac{\tau}{\tau_L}$) this model reduces to the Maxwell model

$$\dot{\gamma} = \frac{1}{G_\infty}\frac{d\tau}{dt} + \frac{\tau}{\mu} \qquad (2a)$$

where the viscous term is classical Newtonian behavior. The limiting case of a visco-plastic liquid results from specifying a small visco-elastic relaxation time $\frac{\mu}{G_\infty}$, so the model takes on the non-linear viscous form of

$$\dot{\gamma} = + \frac{\tau_L}{\mu} \tanh^{-1}\left(\frac{\tau}{\tau_L}\right) \qquad (2b)$$

where

$$\mu = \mu_0 \exp(\alpha \cdot p)$$

and

$$\tau_L = \tau_{L_0} + mp \quad .$$

It is this form which is used in this analysis. The magnitude of the neglected elastic term in the resulting flow is small as will be seen.

B. Derivation of the Governing Equations

Three basic equations are used in an EHD Grubin-type inlet analysis. They are shear constitutive equation (2b), the equation of motion and conservation of mass. Because we assume isothermal conditions throughout, the energy equation is not required. The equations of elasticity are not required because the inlet film shape is assumed to be known from the Hertzian contact analysis.

The details of the derivation are presented in Appendix B, the resulting governing equations are:

$$u_{21} - u_{11} = \left(\frac{\tau_L^2}{2\mu p'}\right) \left[(1 + \hat{r}_2)\ell n(1 + \hat{r}_2) - (1 + \hat{r}_1)\ell n(1 + \hat{r}_1) + (1 - \hat{r}_2)\ell n(1 - \hat{r}_2) - (1 - \hat{r}_1)\ell n(1 - \hat{r}_1)\right] \quad (3\text{-a})$$

$$\frac{u_{21} + u_{11}}{2} h_o = u_{11}h + \left(\frac{\tau_L^2}{2\mu p'}\right) \left\{ \frac{\tau_L}{2p'} \left[(1 + \hat{r}_2)^2(\ell n(1 + \hat{r}_2) - 1/2) - (1 + \hat{r}_1)^2(\ell n(1 + \hat{r}_1) - 1/2)\right] - \frac{\tau_L}{2p'} \left[(1 - \hat{r}_2)^2(\ell n(1 - \hat{r}_2) - 1/2) - (1 - \hat{r}_1)^2 (\ell n(1 - \hat{r}_1) - 1/2)\right] - (1 + \hat{r}_1)h\ell n(1 + \hat{r}_1) - (1 - \hat{r}_1)h\ell n(1 - \hat{r}_1) \right\} \quad (3\text{-b})$$

From Equation 4A $\tau_2 = p'h + F(x_1)$ and $F(x_1) = \tau_1(x_1)$. Since many terms in Equations (3-a) and (3-b) can be expressed as a function of pressure, pressure gradient and x_1, these two equations supposedly could be put in the form of a simple first order ordinary differential equation. But since it is apparently impossible to achieve this form by making elementary algebraic manipulations; equations (3-a) and (3-b) are solved numerically.

The film thickness equation used in the inlet region is $h = h_o + h_s$ where

$$h_s = \frac{a^2}{2R_e}\left\{\left|\frac{x_1}{a}\right|\left[\left(\frac{x_1}{a}\right)^2 - 1\right]^{1/2} - \ln\left[\left|\frac{x_1}{a}\right| + \left[\left(\frac{x_1}{a}\right)^2 - 1\right]^{1/2}\right]\right\} \quad (4)$$

for $\left|\frac{x_1}{a}\right| \geq 1$, and h_o is the nominal EHD film thickness. This is the equation of elastic deformation outside the Hertzian contact, due to the pressure only in the Hertzian contact, which is, for heavily loaded contacts, near Hertz pressure distribution [18].

C. Method of Solution

The two governing equations derived above, Equations (3-a) and (3-b), are solved numerically, for the two unknowns p' and τ_1. Since some terms are functions of pressure, the solution method can be described as the solution of two nonlinear equations along with the solution of the differential equation (Equation 5), to find the pressure distribution in the inlet zone.

The solution starts in the inlet at x_1 where the film thickness h is ten times greater than the nominal film thickness h_o. Based on starvation analysis of contacts [19], it is reasonable to exclude the region where $h > 10\ h_o$, and perform the film thickness analysis in the region $h \leq 10\ h_o$. The value of x_1 at this point is found from the film thickness equation (4) for each given set of operating conditions and h_o. At this point pressure is assumed to be zero, and the two non-linear equations are solved numerically for p' and τ_1. With these initial conditions of p' and p, Equation (5) is solved numerically, to predict the pressure at the next grid point. This process continues up to the point where $x_1 = a$, the Hertz contact radius. The distance between the initial x_1 value and the final value of x_1 is uniformly divided into two hundred steps (Δx_1). Increasing the number of grid points gives more accuracy but at the same time consumes more computing time. Based on the observation of a few runs of the program it appears that the number of grid points has little influence when increased from 200 to 500.

The IMSL library subroutine "ZSYSTM" was used for the solution of the two non-linear equations. At each grid point the solution of the previous point is used as the initial guess value. Euler's method is used for the solution of the differential equation

$$p_{i+1} = p_i + \Delta x_1 \, p_i' , \qquad i = 1,n \qquad (5)$$

where n is the number of grid points.

The flow-chart showing the solution scheme is given in Figure 20. As seen in the flow-chart, when τ_1 and τ_2 reach 0.9 times τ_L, the governing equations are modified.

Program Logic, Description of the Computing Procedure

For each set of given physical input data including the nominal film thickness h_o, the program calculates the pressure distribution in the inlet zone including the inlet pressure p_i (at $x_1 = a$, i.e., $h = h_o$). The nominal film thickness depends slightly on the inlet pressure at high inlet pressures and this dependence decreases as the inlet pressure increases. Therefore, h_o tends to an asymptotic value, on h_o versus p_i curves for a given set of operating conditions (U,W,G). The first step in this analysis obtains h_o versus p_i curves by varying h_o for each set of physical input data. Starting h_o values are slightly greater than Grubin's prediction for nominal film thickness, and decreased by small amounts, until the computer program "dumped" because of the logarithmic functions in Equations (3-a) and (3-b). It is clear from the physical situation that decreasing the nominal film thickness is equivalent, in a sense, to increasing pressure (and pressure gradient).

Since the shear stress is directly related to the pressure gradient, these increased pressure gradients will, eventually, cause the shear stress to reach the limiting value. Therefore, the argument of some of the logarithmic functions in Equations (3-a) and (3-b) approach zero. The "dumping" of the computer program dictates a limit to the decrease of h_o, which actually comes from the rheological model as $\hat{\tau}_1$ and $\hat{\tau}_2$ approach unity. In the integrated momentum equation, Equation (4A) the product (p'h) is always positive, therefore $|\tau_2|$ is always greater than $|\tau_1|$. A physical justification for this is to run the upper surface faster.

Consequently, it is expected that τ_2 will approach τ_L before τ_1. In order to handle this difficulty in the numerical solution we impose the criteria that when $\tau_2 \geq 0.9\ \tau_L$ (and $\tau_1 < 0.9\ \tau_L$) a modified version of the governing equations (3-a) and (3-b) are solved where $(1 - \hat{\tau}_2)^n \ln(1 - \hat{\tau}_2)$, n = 1,2 terms are omitted based on the limit identity

$$\lim_{x \to 0} x^n \ln(x) = 0$$

If then $\tau_1 \geq 0.9\ \tau_L$ (and $\tau_2 \geq 0.9\ \tau_L$), we impose the condition $\frac{dp}{dx_1} = 0$ (i.e., p constant), as required by the integrated momentum equation, Equation (4A). Imposing p' = 0 will be discussed later in the discussion section. If both τ_1 and τ_2 approach τ_L, then p' approaches zero, provided that h is nonzero. Although the numerical problem of "dumping" due to the logarithmic functions is handled in this manner drastic decreases in h_o still do not occur.

The operating value of h_o predicted from the analysis is the h_o where $p_i \geq 100$ MPa (15 kpsi) and $\frac{dh_o}{dp_i}$ approaches zero from plots like those shown in Figures 2 and 3.

D. Physical Input Data

The input data employed in the analysis are shown in Tables I through IV. The lubricant properties are representative of typical lubricants at 40C.

Table I. Lubricant and Contact Material Properties

μ_o/mPas (lb/sec/in^2)	410 (5.94×10^{-5})
	41 (5.94×10^{-6})
α/GPa^{-1} (psi^{-1})	32 (2.18×10^{-4})
τ_{L_o}/MPa(psi)	6.9 (1000)
	0.69 (100)
n/dimensionless	0.1
	0.05
R/mm (in.)	12.7 (0.5)
Contact material	Steel on steel

Table II. Load and Hertz Pressure

$\frac{W}{L} / \frac{kN}{m}$ (lb/in)	87.6	(500)
p_H/GPa (kpsi)	0.5	(72.7)
$\frac{W}{L} / \frac{MN}{m}$ (lb/in)	8.76	(5×10^4)
p_H/GPa (kpsi)	5	(727)

Table III. Surface Sum Velocities

(slide/roll ratio Σ is assigned 0, 1, and 2 at each rolling speed.)

$(u_{11} + u_{21}) / \frac{m}{s}$	$(u_{11} + u_{21}) / \frac{in}{s}$
0.254	10
2.54	100
5.0	200

Table IV. Dimensionless EHD Variables [20]

U	3.96×10^{-12}	7.92×10^{-11}	3.96×10^{-10}
W	3×10^4		3×10^2
G	6.54×10^3		

E. Results

h_o versus p_i curves

Figure 21 shows the effect of slide/roll ratio, Σ, on the film thickness inlet pressure relation, for the physical input shown.

For large h_o (i.e., small p_i), change of Σ does not have much effect on the inlet pressure. Although it is not shown in this figure, the solution of Reynold's equation with a Newtonian fluid as used by Grubin approaches these three curves at low inlet pressure values. For inlet pressures around 130 MPa (20 kpsi) or higher this relation reduces to h_o independent of p_i. A straight line shown in Figure 21 represents this Grubin film thickness. At different inlet pressure ranges, all three curves tend to go to an asymptotic h_o value. As shown in the figure, increasing Σ reduces the film thickness.

In Figure 22, the effect of limiting shear stress properties on film thickness is shown. The physical input is the same as in the previous figure, with $\Sigma = 2$ except for τ_{L_o} and m as indicated. The effect of increasing τ_{L_o} and/or m is qualitatively the same as the effect of decreasing Σ. τ_{L_o} and m can be varied independently but their effect will always be in the same direction.

The Shear Stress Distribution

The shear stress distributions in the inlet zone shown in Figure 23 are for the operating conditions represented by the point B in Figure 2. Notice that both τ_1 and τ_2 are below the τ_L values throughout the inlet zone.

In the case of a decreased h_o (i.e., increased p) the shear stress distribution is shown in Figure 24 for the conditions represented by point A in Figure 21, where both $\frac{\tau_1}{\tau_L}$ and $\frac{\tau_2}{\tau_L}$ are around unity. This point is chosen as the point defining h_o predicted by our analysis at which the contact will operate under the given physical input. The pressure gradient (See Figure 28) is zero near the inlet (pressure constant, see Figure 29), and h_o tends to go to an asymptotic value at inlet pressures around 100 to 130 MPa (15 to 20 kpsi).

The shear stress distribution under pure rolling (point C of Figure 21) is shown in Figure 25. Notice the signs and behavior of τ_1 and τ_2 both of which approach zero near the entrance to Hertz contact resulting in a zero pressure gradient at that point.

Pressure Gradient and Pressure Distribution

Figure 26 represents the conditions denoted by point B in Figure 21. The related pressure distribution is given in the Figure 27. In Figure 28, the p' distribution for the conditons represented by point A of Figure 21 is shown. Notice the increase in the p'_{max} value compared with that in Figure 26 (although not by order of magnitude due to the fact that h_o values does not differ much) and the movement of the peak to the right. The pressure distribution for this case is given in Figure 29.

Pressure gradient and pressure distributions under pure rolling condition are shown in Figures 30 and 31, for the conditions represented by the point C of Figure 21 (point C, where p_i is around 260 MPa, is out of the range of the Figure 21). The p'_{max} value is greater than the one shown in Figure 26 by one order of magnitude. The related pressure

distribution is shown in Figure 31. This resembles Grubin's infinite inlet pressure condition.

H_o versus U, and H_o versus W curves

Figure 32 shows the dependency of H_o on U for w/L = 87.6 kN/m(500 lb/in) (p_H = 0.5 GPa = 72 kpsi), with the material property G = 6540, and for two different slide/roll ratios. μ_o and u are varied in the range displayed in the previous tables to maintain the indicated U values [See Table IV]. The limiting shear stress parameters are kept constant. Qualitatively, since the effect of changing the limiting shear stress parameters is the same as changing the slide-roll ratio (See Figures 21 and 22), these variations are not shown on H_o versus U curves. The conditions for Figure 33 differ from those in Figure 32 only in that the load is, w/L = 8.76 MN/m (5×10^4 lb/in) (or p_H = 5 GPa = 727 kpsi). The data in Figures 32 and 33 are plotted in Figure 34 to show the dependence of the film thickness on load which is only slightly changed from the classical Grubin result. (Note that limiting shear stress parameters τ_{L_o} = 0.69 MPa m = 0.05; and the material parameter G = 6540 remain unchanged in Figures 32, 33 and 34.)

F. Discussion

The basic equations employed: Only the visco-plastic portion of the constitutive equation, Equation 2 was used. By examining the results, the assumption of omitting the elastic term of that equation appears to be justified. The results presented permit the following order or magnitude analysis:

$$\Delta\tau \cong 0.7 \text{ to } 7 \text{ MPa } (10^2 \text{ to } 10^3 \text{ psi})$$

$$\Delta x_1 \simeq 0.25 \text{ to } 0.025 \text{ mm } (10^{-2} \text{ to } 10^{-3} \text{ in})$$

$$\tilde{u} = \frac{u_{21} + u_{11}}{2} \cong 0.25 \text{ to } 2.5 \text{ m/s } (10 \text{ to } 10^2 \text{ in/s})$$

and for the typical pressure range encountered,

$$G_\infty \cong 0.7 \text{ GPa } (10^5 \text{ psi})$$

$$\tau_L \simeq 0.7 \text{ to } 7 \text{ MPa } (10^2 \text{ to } 10^3 \text{ psi})$$

$$\mu \simeq 0.7 \text{ to } 7 \text{ Pas } (10^{-4} \text{ to } 10^{-3} \text{ lbs/in}^2)$$

and as $\frac{\tau}{\tau_L}$ approaches unity $\tanh^{-1}\left(\frac{\tau}{\tau_L}\right)$ will be at least in the range of 1 to 10 or much greater. Therefore, if we approximate the elastic term in the constitutive equation as

$$\frac{1}{G_\infty}\frac{d\tau}{dt} = \frac{1}{G_\infty}\frac{d\tau}{dx_1}\frac{dx_1}{dt} \simeq \frac{1}{G_\infty}\frac{\Delta\tau}{\Delta x_1}\tilde{u}$$

it will be on the order of 10^0 to 10^3 while the visco-plastic term used will be

$$\frac{\tau_L}{\mu} \tanh^{-1}\left(\frac{\tau}{\tau_L}\right) \simeq 10^5 \text{ to } 10^8$$

or more as $\frac{\tau}{\tau_L}$ approaches unity.

Therefore for the case we deal with in this analysis the elastic term is smaller than the nonlinear viscous term by at least two orders of magnitude due to the fact that the elastic modulus G_∞ is high, and viscosity is low. Consequently, it is reasonable to omit the elastic term of the constitutive equation in this inlet analysis. This assumption may not be valid for an analysis which considers the Hertzian contact zone where pressure (therefore viscosity) is much higher than it is at the inlet zone.

The assumption of an isothermal flow condition can be justified for the rolling case by using the results of Murch and Wilson [21] and Cheng [22]. Their thermal reduction factor ϕ_T is available, which can be multiplied with the isothermal calculation of h_o, to find the actual h_o. For our high viscosity case using a thermal conductivity of mineral oil 0.12 W/m-C (0.015 lb/^{o}F-sec) and temperature coefficient of $0.04C^{-1}$ ($0.02\ F^{-1}$), ϕ_T will be 0.9 or higher where u = 200 in/sec or smaller. The energy dissipation with our non-linear fluid will be less than the Newtonian fluid they consider for other conditions equal. Hence neglecting the inlet zone heating effects and assuming isothermal condition is valid for the range of variables used.

As stated in the above discussion of the solution technique, when both τ_1 and τ_2 approach the limiting shear stress the pressure gradient was assigned a value of zero. As seen from the integrated momentum equation (Equation 4A), if τ_1 and τ_2 were both equal to the limiting value, the pressure gradient would have to be zero because h is nonzero. However, the shear constitutive equation (2-b) shows the shear stresses only reach the limiting value as the shear rate approaches infinity. Consequently the p'h term of the momentum equation must approach zero and is the difference between two large nearly equal numbers. The numerical difficulties this causes were eliminated by simply forcing p' to zero although it would be small not zero. This step was only required very near the Hertzian inlet zone as the operating film thickness was approached, (See Figure (28)). When p' is set to zero the constitutive equation combined with momentum Equation (5A) would give a constant shear rate across the film, hence a linear velocity profile, which violates continuity because h is not constant outside the Hertzian region. The numerical convenience of forcing p' to zero under these conditions is thought to have no major effect on the conclusions of the analysis and no more important than other assumptions inherent in a Grubin-type solution numerically executed.

The effect of the conventional terms, load, speed and the material parameters, on film thickness is in the same sense as expected in any Grubin type film thickness analysis. For a fixed material parameter G, the dimensionless film thickness H depends slightly upon the load parameter W but is more sensitive to the changes in the speed parameter U

as seen in the Figures 34, 33 and 32 respectively. When the sum velocity approaches zero (or the vsicosity μ approaching zero), the nominal film thickness approaches zero (i.e., dry contact) and the three lines of Figures 32 and 33 approach each other for smaller film thicknesses.

The effect of increasing the limiting shear stress parameters, τ_{L_o} and m, as shown in Figure 32 is to cause the model to give results close to the results of the Newtonian model. When either τ_{L_o} or m (or both) is increased the resulting τ_L value at that particular point is increased, hence the term $\frac{\tau}{\tau_L}$ is decreased and it is less likely to approach unity with increasing $|\tau|$. The behavior approaches Newtonian viscous behavior and the asymptotic tendency of h_o is therefore to Grubin's predictions.

The τ_{L_o} and m values (at a specified temperature) are available from the experimental our previous studies [2]. Some of the values used in this analysis are approximated from the data on the lubricant 5P4E (polyphenyl ether) at 40C. The importance of the slope m dominates the importance of the zero pressure value τ_{L_o} because near the inlet to the Hertzian contact zone the pressure increases rapidly and τ_L follows this rapid increase through the parameter m. The effect of τ_{L_o} is far out in the inlet zone where the pressure is low and the shear stress is low.

The effect of increasing sliding speed on $\left|\frac{\tau_i}{\tau_L}\right|$, i = 1,2 is qualitatively the same as the effect of decreasing the limiting shear stress parameters. Apparently this effect is not altered by the rolling speed at which the sliding is increased. Decreasing the slide-roll ratio

(or increasing the limiting shear stress parameters) increases the h_o value predicted by this analysis, and shifts this asymptotic value to the right on h_o versus p_i curves. This is due to the fact that at low slide/roll ratios and/or with high limiting shear stress parameters the lubricant behaves like a Newtonian fluid and therefore at the asymptotic value of h_o, higher pressures (and pressure gradients) are possible to achieve.

The effect of the lubricant viscosity can be analyzed in the same sense as the effect of the sliding speed, since increase in either one will cause the shear stress to increase. It was observed from a few solutions of the model that for materials like some silicone fluids with extremely high μ_o values and low τ_L values the shear stresses on the surfaces reach the limiting value even at unreasonably high h_o values although pressure and pressure gradients are low. With this type of lubricant our assumption of omitting the elastic term from the constitutive equation may not be valid. The high viscosity lubricants work with high limiting shear stress parameters and low slide/roll ratios, if they work at all.

G. Conclusions

This analysis confirms the idea that when the shear stress reaches the limiting value in the inlet zone there will be a reduction in the nominal film thickness. This reduction, for most conventional lubricants, is not drastic. For the slide/roll ratio value of two, it is found that the nominal film thickness is about thirty to forty percent less than Grubin's prediction when the dimensionless film thickness, H, is in the order of 10^{-4}; and about twenty percent or less reduction is predicted when the film thickness is in the order of 10^{-5} or less.

The slide/roll ratio, and the lubricant limiting shear stress are the two newly introduced concepts in a Grubin type film thickness analysis. Decreasing the slide/roll ratio and/or increasing the limiting shear stress parameters resulted in Newtonian-like behavior. This characteristic behavior is implied in the non-linear visco-plastic rheological model.

Although the confirmation of the existence of a limiting shear stress is relatively new in the field of tribology, it is an intrinsic material property of the lubricants that have been used for many years. Therefore it is reasonable to expect as concluded that, under usual operating conditions, with conventional lubricants, no drastic changes or sudden collapse in film thickness is expected. Hence the small ($\lesssim$ 40 percent) reduction in film thickness predicted in this analysis is reasonable.

REFERENCES

1. Winer, W. O., and Sanborn, D. M., "Surface Temperatures and Glassy State Investigations in Tribology", NASA CR-3031, (June 1978).

2. Winer, W. O. and Bair, S. S., "Investigations of Lubricant Rheology as Applied to EHD Lubrication", NASA (June 1978).

3. Harrison, G., The Dynamic Properties of Supercooled Liquids, Academic Press (1976).

4. Smith, F. W., "Lubricant Behavior in Concentrated Contact Systems--The Castor Oil-Steel System", Wear 2, No. 4, (1959) 260-263.

5. Plint, M. A. M., "Traction in Elastohydrodynamic Contacts", Proc. Inst. Mech. Engrs., 182, Part 1 (1967-68) 300-306.

6. Johnson, K. L., and Roberts, A. D., "Observations of Viscoelastic Behavior of an Elastohydrodynamic Lubricant Film", Proceedings of the Royal Society of London, 337A, (1974) 217-242.

7. Johnson, K. L., and Cameron, R., "Shear Behaviour of Elastohydrodynamics Oil Films at High Rolling Contact Pressures", Proc. Inst. Mech. Engrs., 182, Part 1 (1967-68) 307-319.

8. Johnson, K. L., and Tevaarwerk, J. L., "Shear Behaviour of Elastohydrodynamic Oil Films", Proc. Roy. Soc. of London, 365A, (1977) 215-236.

9. Bair, S., and Winer, W. O., "Shear Strength Measurements of Lubricants at High Pressure", ASME Paper No. 78-LUB-8, (to be published Journal of Lubrication Technology (1979)).

10. McKinny, J. E., and Goldstein, M., "PVT Relationships for Liquid and Glassy Poly(Vinyl Acetate)", Journal of Research of the NBS-Physics and Chemistry, 78A, (1974) 331.

11. Nagaraj, H. S., and Winer, W. O., "Surface Temperature Measurements in Rolling and Sliding EHD Contacts", to be published in ASLE Trans., ASLE Paper No. 78-AM-2B-2.

12. Haward, R. N., The Physics of Glassy Polymers, New York, Wiley and Sons, Inc.

13. Kalker, J. J., Proc. K. Ned. Akad. Wet., B67, p. 135.

14. Gecim, B., "Elastohydrodynamic Inlet Zone Analysis for Viscoplastic Lubricants", M. S. Thesis, Georgia Institute of Technology, April 1979.

15. Aggrawal, B. B., and Wilson, W. R. D., "A Plastohydrodynamic Inlet Zone Analysis for a Viscoplastic Lubricant", Wear 47, 1978, 119-132.

16. Bell, J. C., "Lubrication of Rolling Surfaces by a Ree-Eyring Fluid", ASLE Transactions 5, (1962) 160-171.

17. Bell, J. C. and Kannel, J. W., "Interpretations of the Thickness of Lubricant Films in Rolling Contact", Influence of Possible Rheological Factors", ASME Transactions, Journal of Lubrication Technology, Paper No. 71-Lub-T (1971) 485-497.

18. Cameron, A., The Principles of Lubrication, John Wiley and Sons, Inc., (1966).

19. Wedeven, L. D., "Effect of Starvation on Film Thickness and Traction under Elastohydrodynamic Rolling and Sliding Conditions", NASA TN D-8087 (October 1975).

20. Dowson, D., and Higginson, G. R., The Fundamentals of Roller Gear Lubrication Elasto-hydrodynamic Lubrication, Pergamon Press, 1966.

21. Murch, L. E., and Wilson, W. R. D., "A Thermal EHD Inlet Zone Analysis", ASME Trans., Journal of Lubrication Technology, 97, Series F. No. 2, April 1975, pp. 212-216.

22. Cheng, H. S., "Calculation of EHD Film Thickness in High Speed Rolling and Sliding Contacts", MTI Report, MTI 67TR24, (May 1967).

APPENDIX A

DESCRIPTION OF EXPERIMENTAL FLUIDS

Symbol:	N1	
Source:	Sun Oil Company	
Type:	Naphthenic Base Oil R-620-15	
Properties:	Viscosity at 37.8C, m^2/s	24.1×10^{-6}
	Viscosity at 98.9C, m^2/s	3.73×10^{-6}
	Viscosity Index (ASTM D-2270)	-13
	Flash Point, C	157
	Pour Point, C	-43
	Density at 20C, Kg/m^3	915.7
	Average Molecular Weight	305

Symbol:	MCS-460	
Source:	Monsanto Company	
Type:	Synthetic Hydrocarbon	
Properties:	Viscosity at 37.8C, m^2/s	37.2×10^{-6}
	Viscosity at 98.9C, m^2/s	4.0×10^{-6}
	Viscosity at 148.9C, m^2/s	1.9×10^{-6}
	Pour Point, C	-29 to -32
	Density 25C, Kg/m^3	932.7

Symbol:	Santotrac 50	
Source:	Monsanto Company	
Type:	Synthetic Cycloaliphatic Hydrocarbon Traction Fluid	
Properties:	Viscosity at 37.8C, m^2/s	34×10^{-6}
	Viscosity at 98.9C, m^2/s	5.6×10^{-6}
	Pour Point, C	-37
	Density at 37.8C, Kg/m^3	889
	Flash Point, C	163
	Fire Point, C	174
	Specific Heat at 37.8C, J/Kg·K	2332
	Additive package includes: Antiwear (zinc dialkyl dithiophosphate), Oxidation inhibitor, Antifoam, VI Improver (Polymethacrylate).	

Symbol:	5P4E	
Type:	Five-ring Polyphenyl Ether	
Source:	Monsanto Company	
Properties:	Viscosity at 37.8C, m^2/s	363×10^{-6}
	Viscosity at 98.9C, m^2/s	13.1×10^{-6}
	Density at 22.2C, Kg/m^3	1205
	Density at 37.8C, Kg/m^3	1190
	Flash Point, C	288
	Pour Point, C	4.4

Symbol:	N3	
Type:	Blend of N1 and 4% Polyalkylmethacrylate (PL-4523)	
Blend Properties:	Viscosity at 37.7C, m^2/s	182×10^{-6}
	Viscosity at 98.8C, m^2/s	27×10^{-6}
	Pressure viscosity coefficient (atmospheric pressure slope)	
	at 37.7C, GPa^{-1}	10.7
	at 98.8C, GPa^{-1}	8.27
Source of Polymer:	Rohm and Haas Company	
Properties of Polymer:	Viscosity Average Molecular Weight	1.65×10^6
	Viscosity m^2/s at 98.9C	773×10^{-6}
	Consists of 19% Polymer in solution with a paraffinic hydrocarbon	

Symbol:	Krytox 143-AB (Lot 10)	
Type:	Perfluorinated polyether	
Source:	DuPont Company	
Properties:	Viscosity at 37.8C, m^2/s	96.6×10^{-6}
	Viscosity at 98.9C, m^2/s	11.5×10^{-6}
	Density at 24C, kg/m^3	1890
	Density at 98.9C, kg/m^3	1760
	V.I. (ASTM D-2270)	116
	Pour point, C	-40
	Flammability	does not burn

Symbol:	XRM-177-F (Lot 4)	
Source:	Mobil	
Type:	Synthetic Paraffinic Hydrocarbon	
Properties:	Viscosity at 37.8C, Pas	376×10^{-3}
	Viscosity at 98.9C, Pas	31.6×10^{-3}
	Pour Point, C	< -40
	Density 37.8C, Kg/m^3	838.9

APPENDIX B

DERIVATION OF PRESSURE GRADIENT EQUATIONS

The visco-plastic constitutive equation, Equation 2-b, is

$$\frac{du_1}{dx_3} = \frac{\tau_L}{\mu} \tanh^{-1} \left(\frac{\tau_{13}}{\tau_L} \right) \tag{1B}$$

where $\dot{\gamma} = \frac{du_1}{dx_3}$ and $\tau = \tau_{13}$ is the shear stress in the x_1 direction on the surfaces with an outward normal in x_3 direction. The reduced form of momentum equation

$$\frac{\partial p}{\partial x_1} = \frac{\partial \tau_{13}}{\partial x_3} \tag{2B}$$

and the continuity equation

$$\int_{x_3 = 0}^{x_3 = h(x_1)} u_1 dx_3 = Q = \text{constant} \tag{3B}$$

are solved as follows.

Integrating Equation 2B with respect to x_3 gives,

$$\tau_{13} = \frac{dp}{dx_1} x_3 + F(x_1) \tag{4B}$$

where

Then substituting Equation (4B) into Equation (1B) results in

$$\frac{du_1}{dx_3} = \frac{\tau_L}{\mu} \tanh^{-1}\left[\left(\frac{dp}{dx_1} x_3 + F(x_1)\right)/\tau_L\right] \quad . \tag{5B}$$

It is clear from Equation (5B) that for $\frac{dp}{dx_1} = 0$, the velocity u_1 is a linear function of x_3, which with the no slip boundary conditions gives the flowrate $Q = \frac{u_{11} + u_{21}}{2} h_o$. This is the same result as found with the usual Newtonian model [14]. Integrating Equation 5B from surface 1 with respect to x_3 gives the velocity distribution

$$u_1(x_3) - u_{11} =$$

$$= \frac{\tau_L^2}{2\mu p'}\left[\left(1 + \frac{p'x_3 + F}{\tau_L}\right)\ln\left(1 + \frac{p'x_3 + F}{\tau_L}\right) - \left(1 + \frac{F}{\tau_L}\right)\ln\left(1 + \frac{F}{\tau_L}\right)\right.$$

$$\left. + \left(1 - \frac{p'x_3 + F}{\tau_L}\right)\ln\left(1 - \frac{p'x_3 + F}{\tau_L}\right) - \left(1 - \frac{F}{\tau_L}\right)\ln\left(1 - \frac{F}{\tau_L}\right)\right] \tag{6B}$$

If $x_3 = h$, then $u_1 = u_{21}$ and it will be the Equation (3-a) of the text.

Integrating the velocity distribution, Equation (6B), in continuity, Equation (3B) will result in Equation (3-b) of the text.

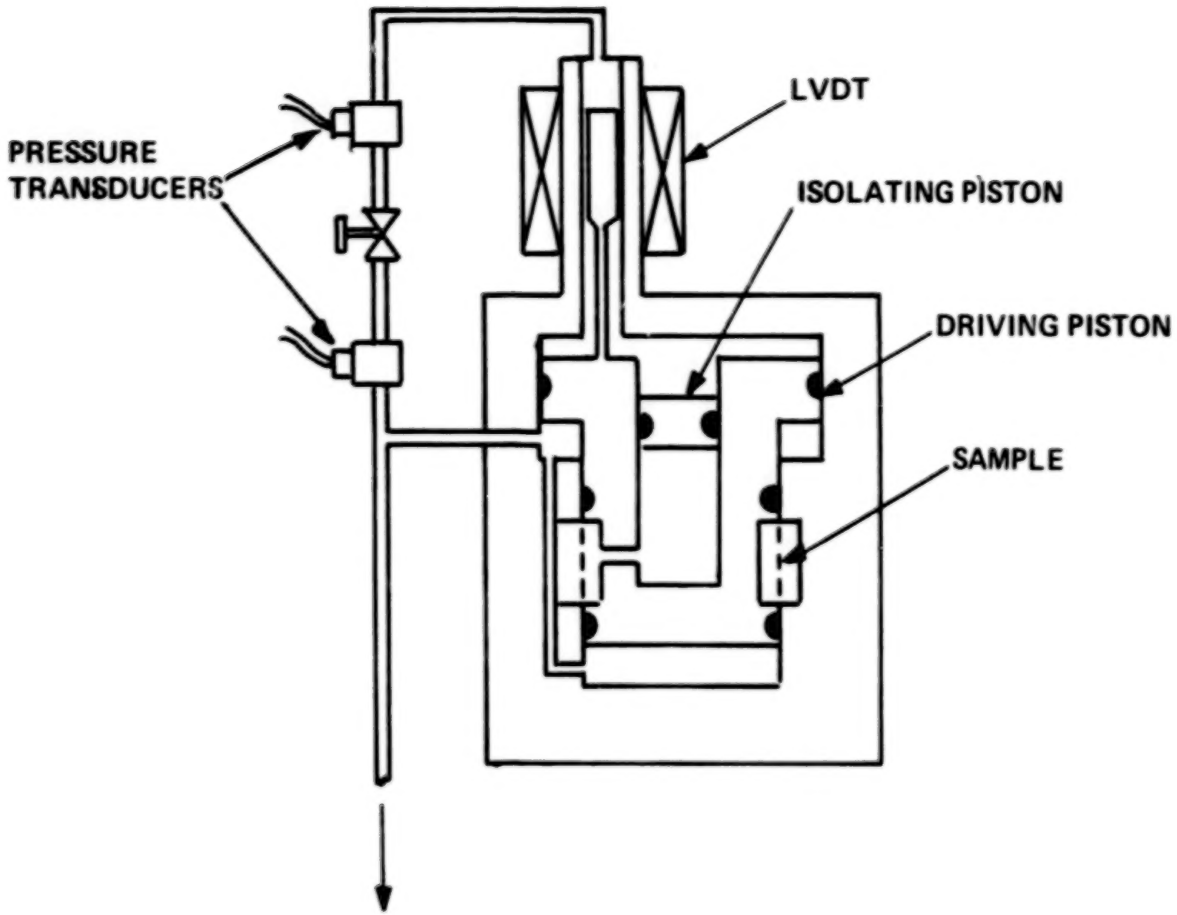

Figure 1. Schematic of Low Pressure Shear Stress Apparatus, 0.7 GPa (100 kpsi)

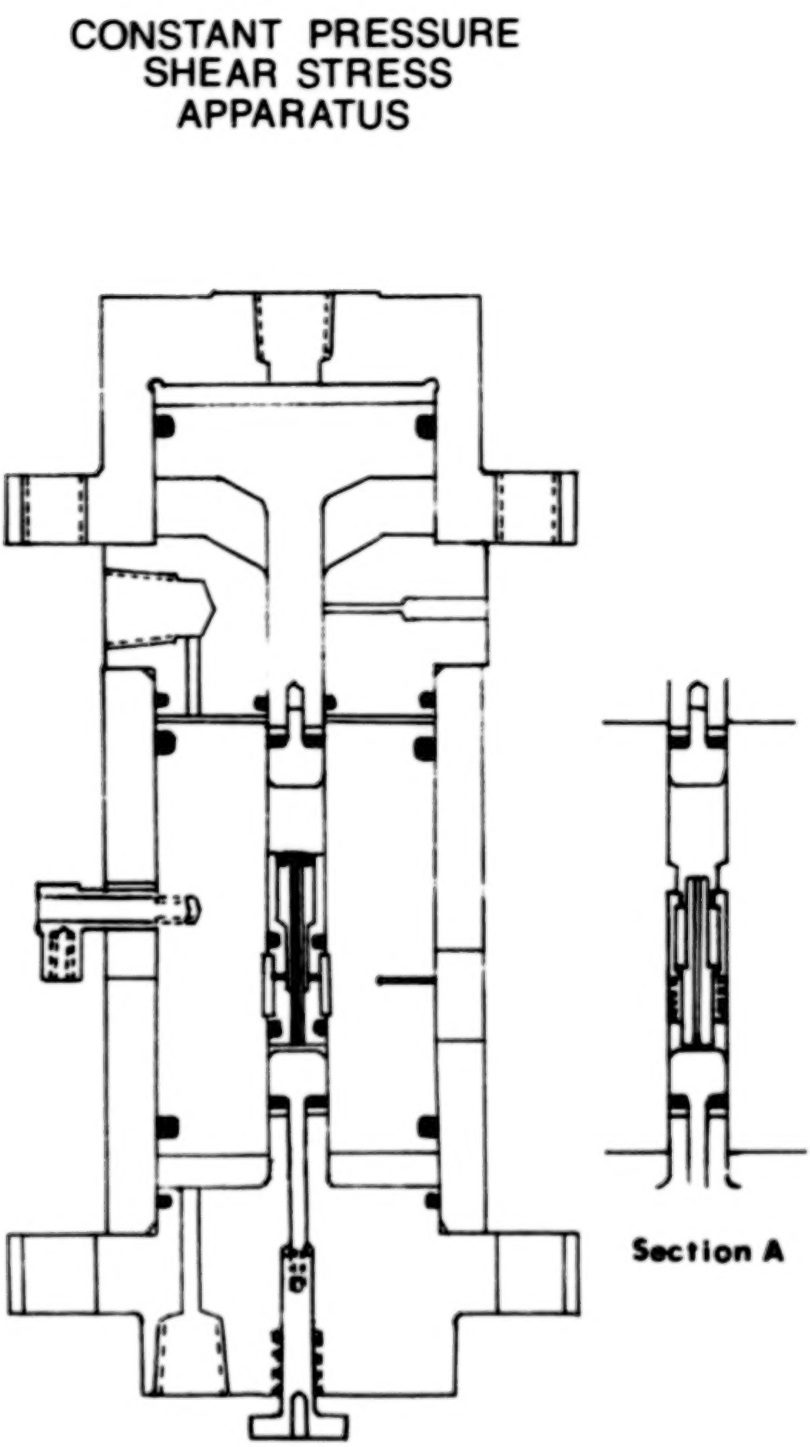

Figure 2. Constant Pressure Stress-Strain Apparatus, 1.1 GPa (Section A: modification for solid sample).

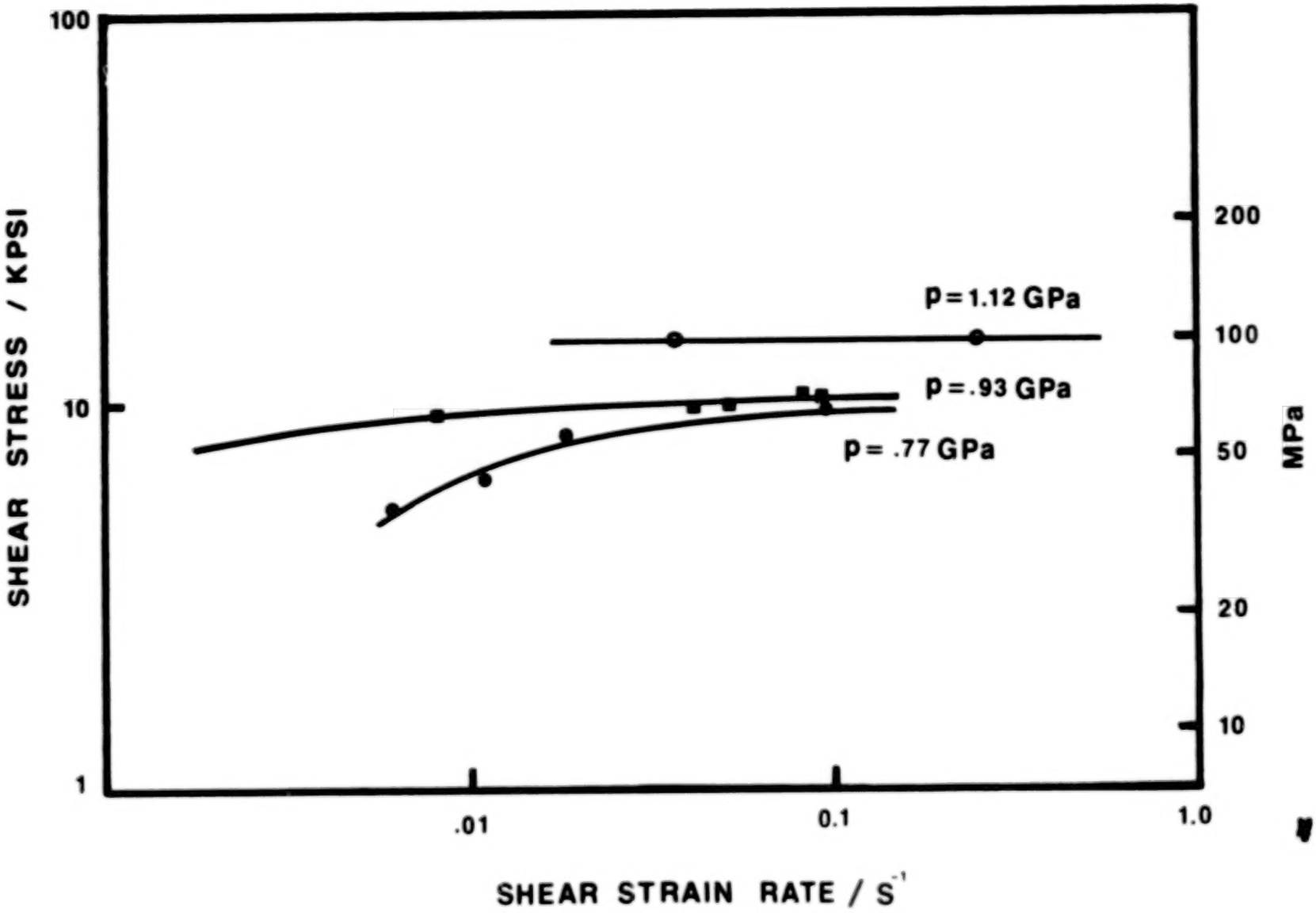

Figure 3. Shear Stress vs. Shear Strain Rate for Ni at 25C

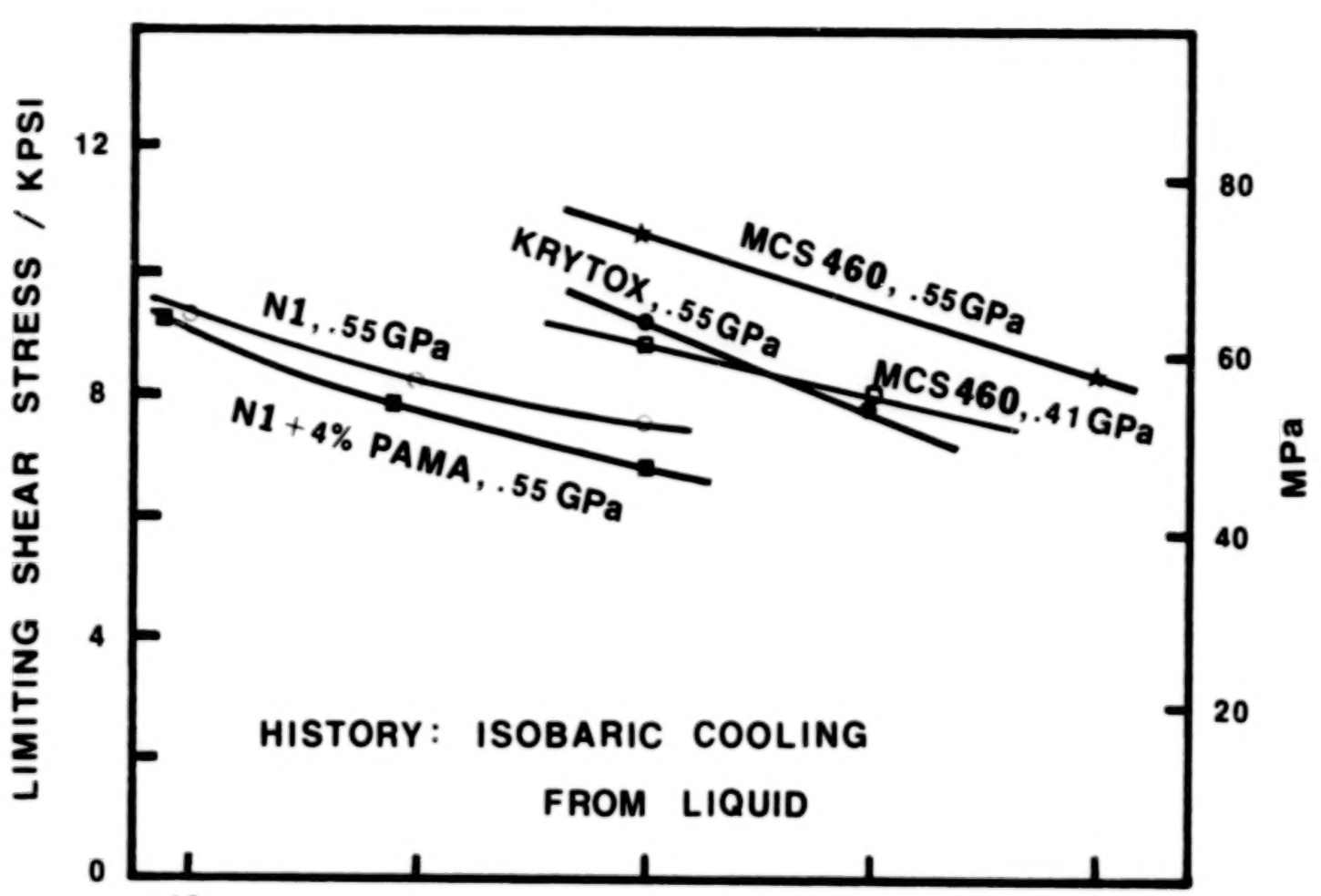

Figure 4. Limiting Shear Stress vs. Temperature for MCS 460, Krytox, N1, and N1 + 4 percent PAMA (Cooling History)

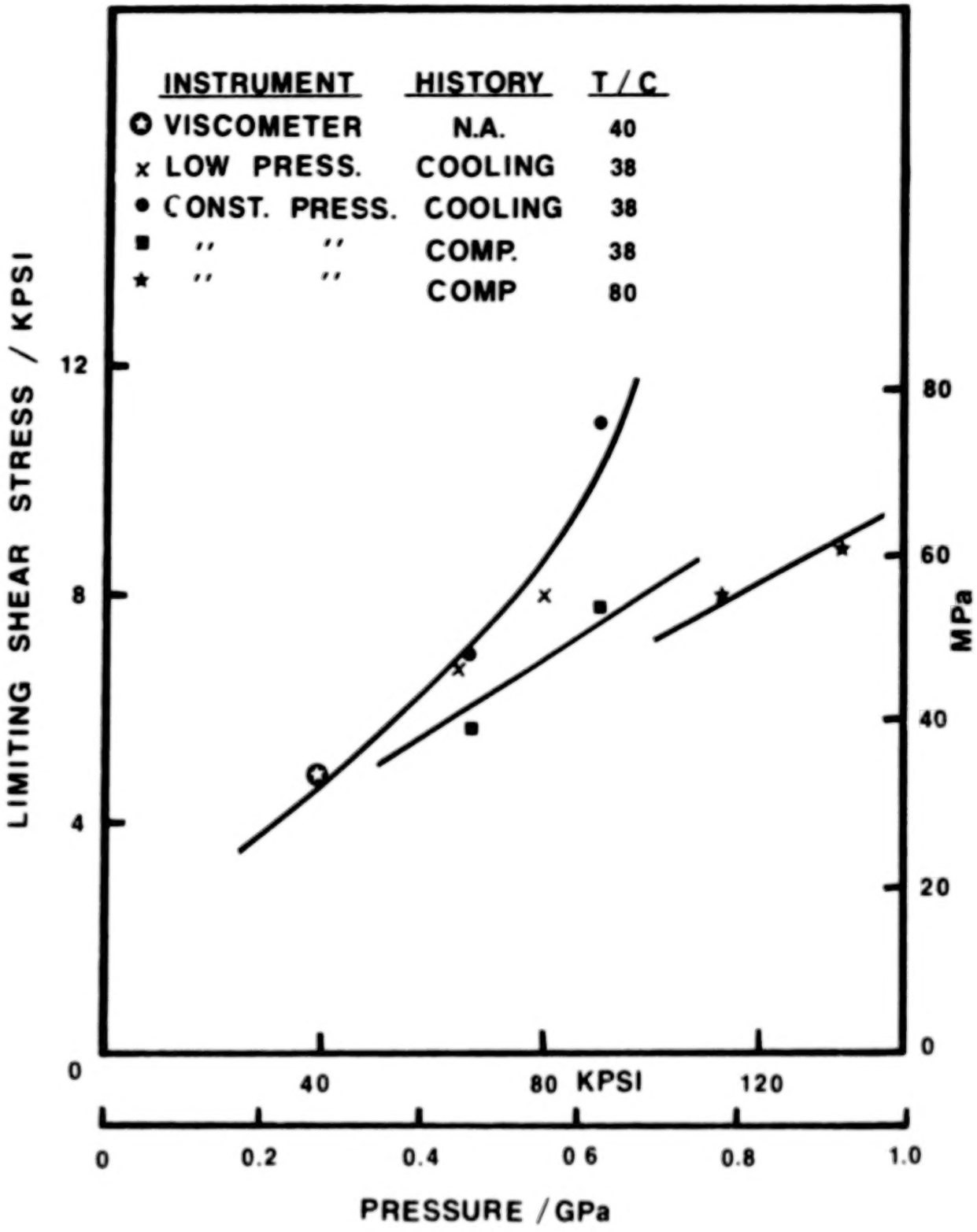

Figure 5. Limiting Shear Stress of 5PHE (polyphenyl ether) vs. Pressure for two Histories and Two Temperature

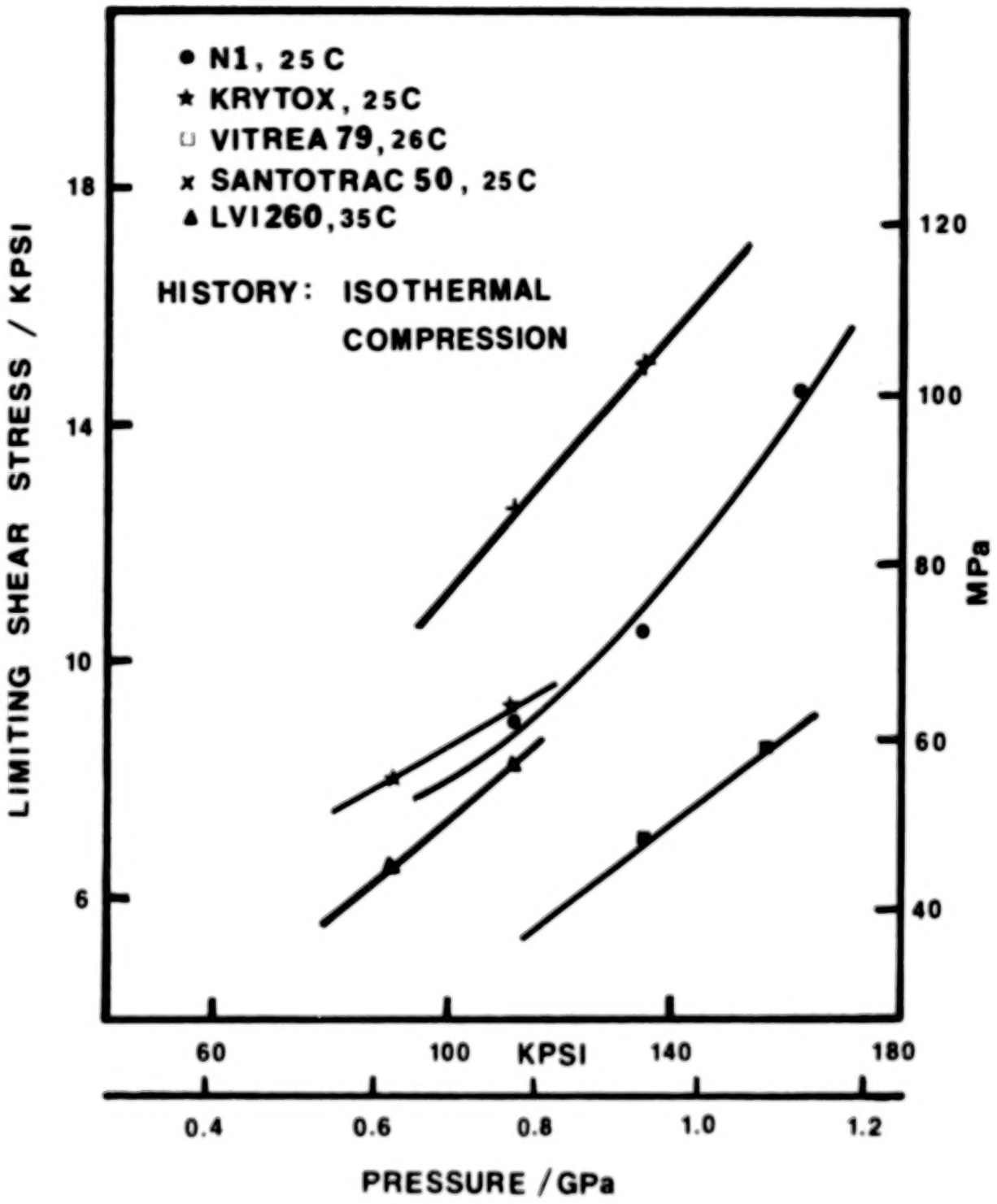

Figure 6. Pressure-τ_L Isotherms for N1 (Naphthenic Base Oil), Krytox (perfluorinated Polyether), Santotrac 50 (Cycloaliphatic Hydrocarbon Traction Fluid)

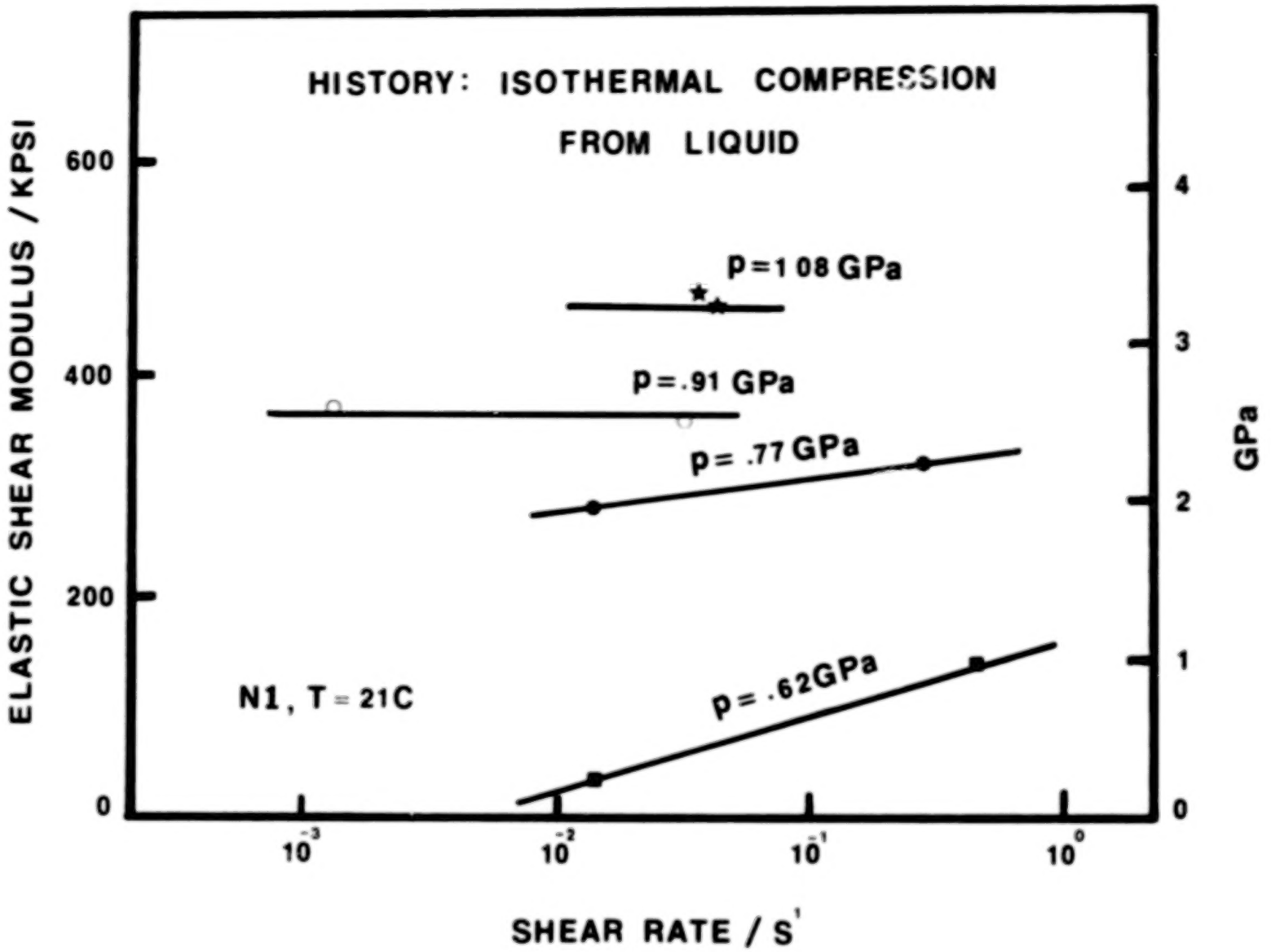

Figure 7. Elastic Shear Modulus of N1 (Naphthenic Base Oil) vs. Shear Rate at Four Pressures and 21C

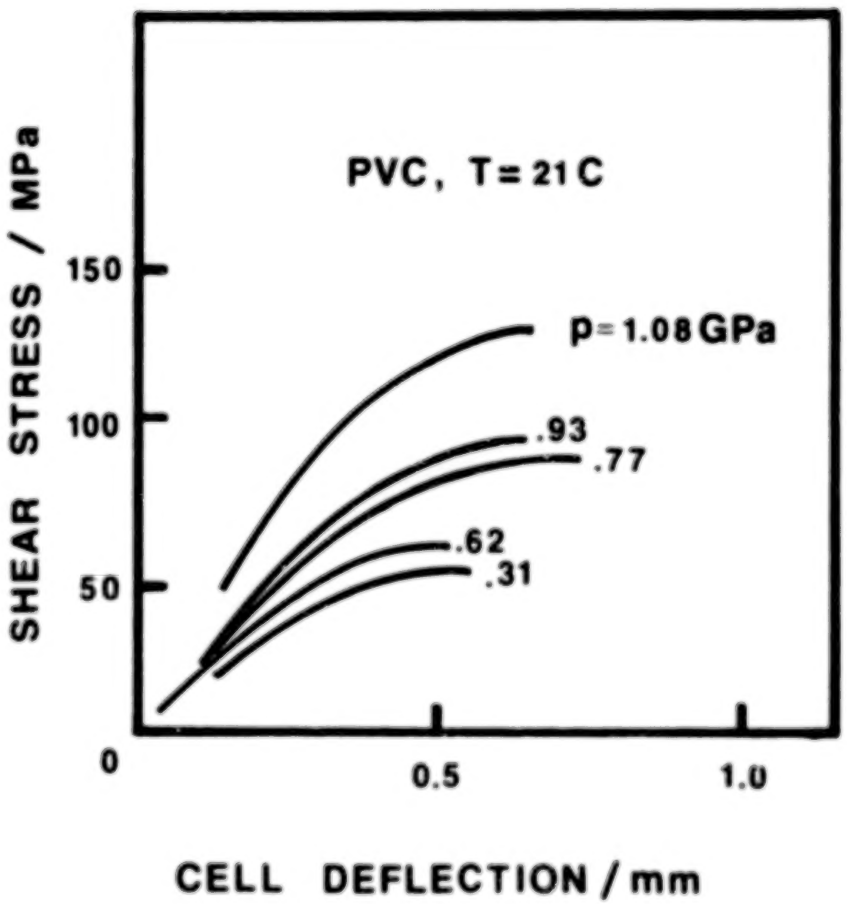

Figure 8. Shear Stress-Cell Deflection for Polyvinyl Chloride at Five Pressures and 21C

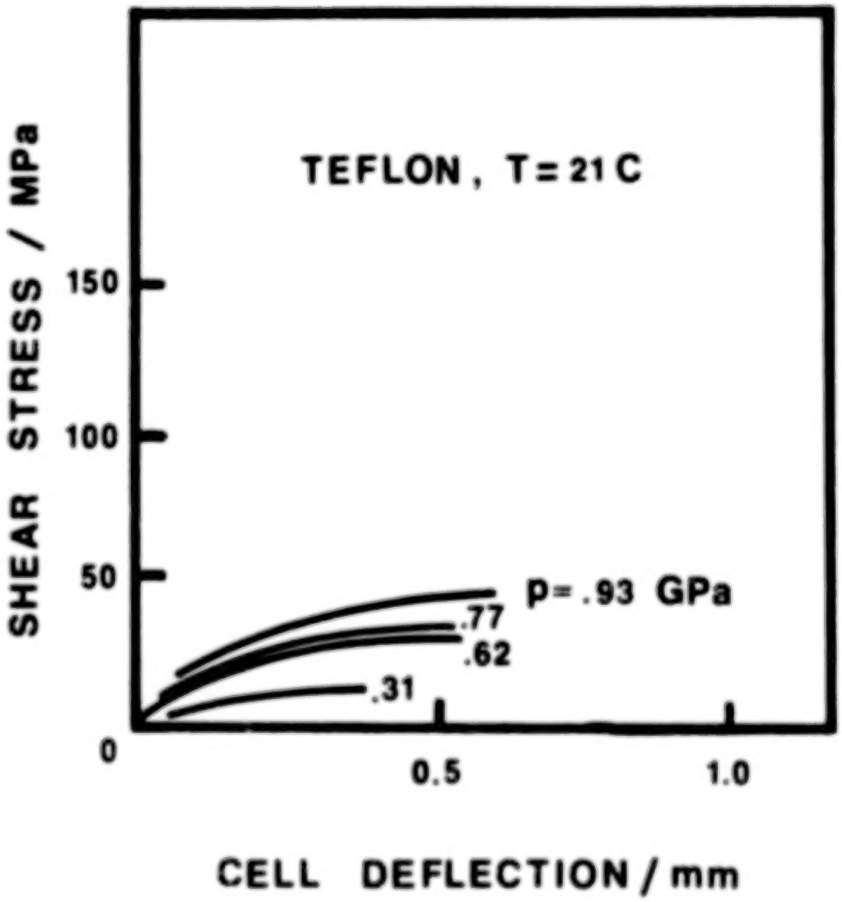

Figure 9. Shear Stress-Cell Deflection for Teflon at Four Pressures and 21C

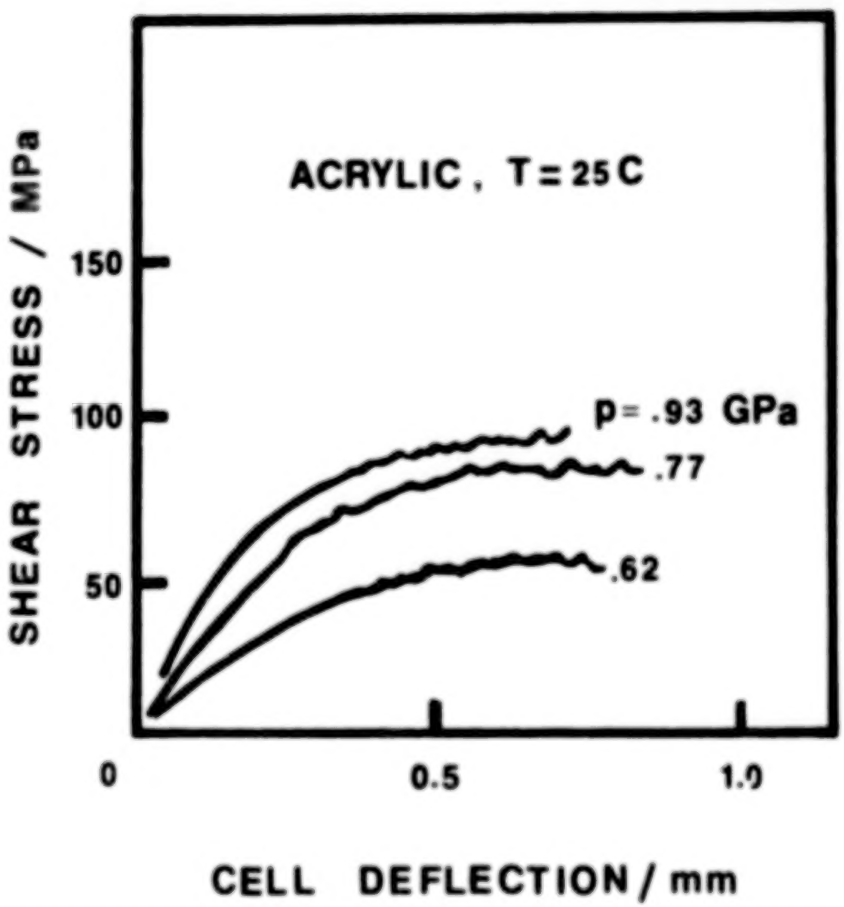

Figure 10. Shear Stress-Cell Deflection for Acrylic Plastic at Three Pressures and 25C

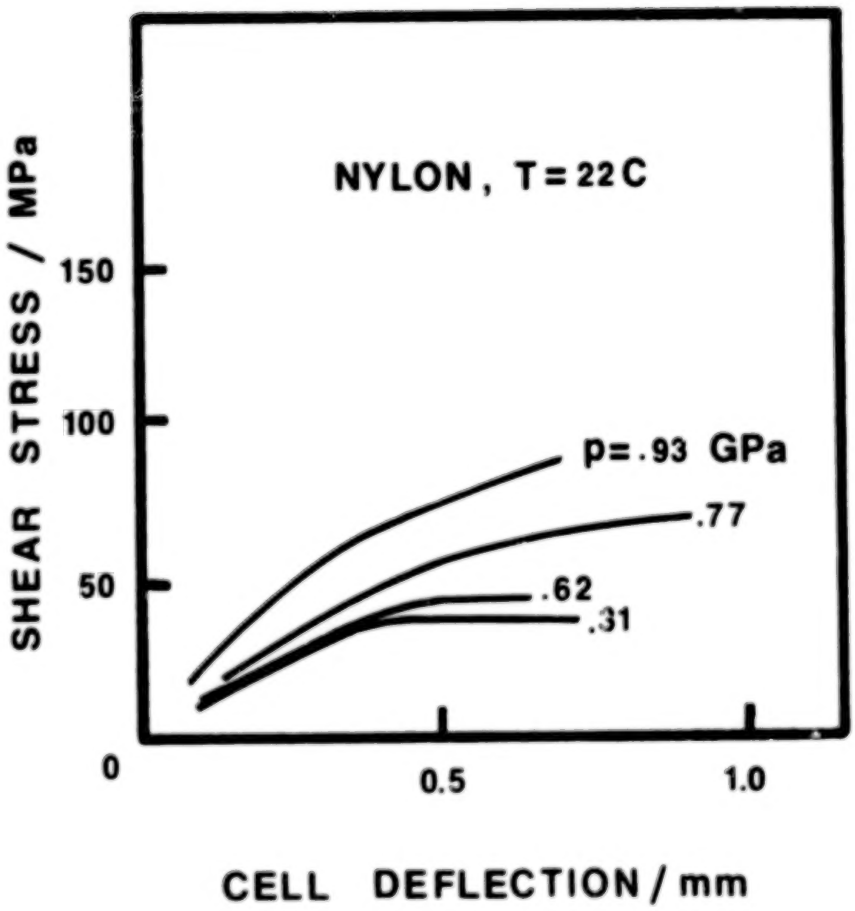

Figure 11. Shear Stress-Cell Deflection for Nylon at Four Pressures and 22C

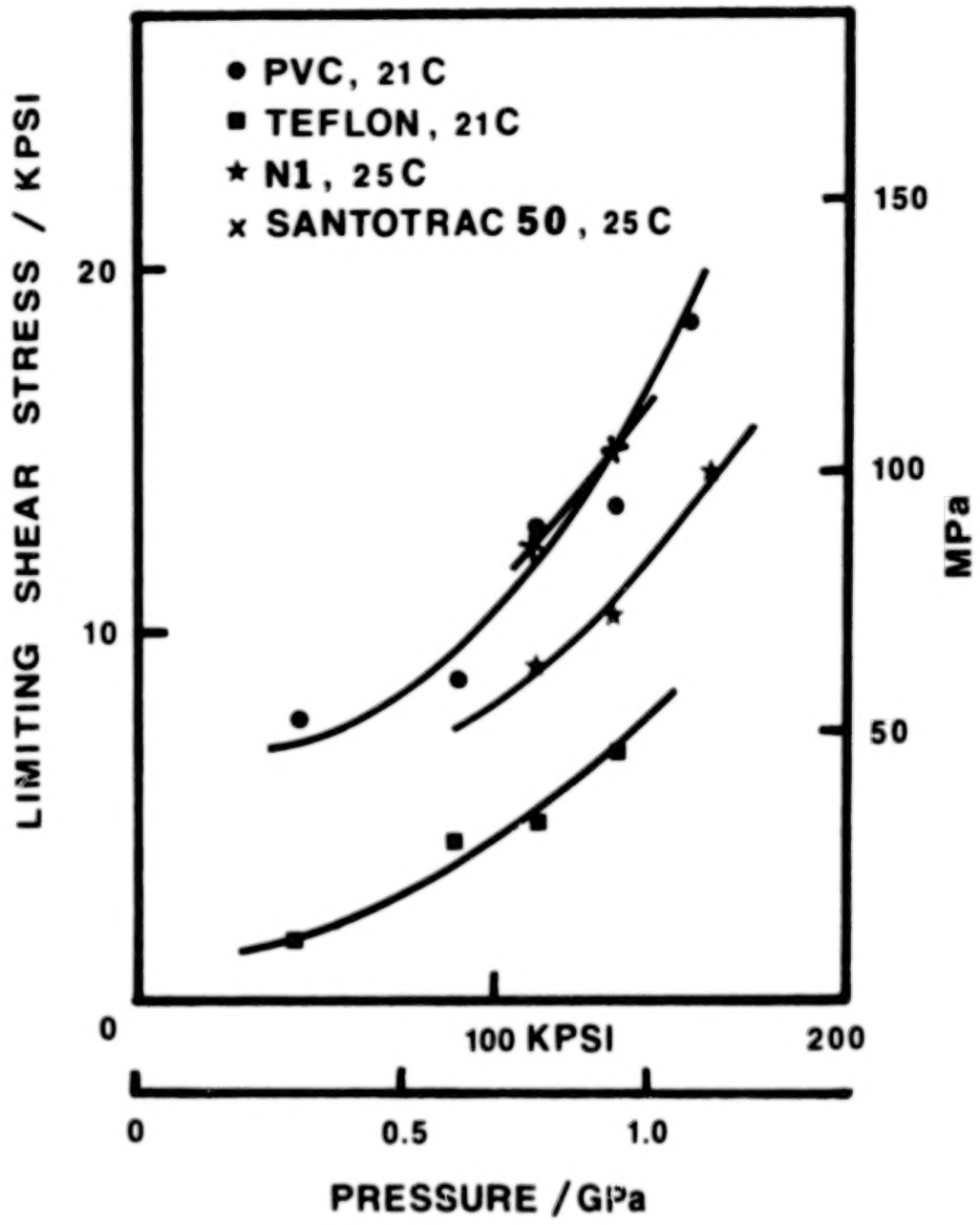

Figure 12. Shear Strength or Limiting Stress vs. Pressure for N1 (Naphthenic Base Oil), Santotrac 50 (Cycloaliphatic Hydrocarbon), Polyvinyl Chloride, and Teflon

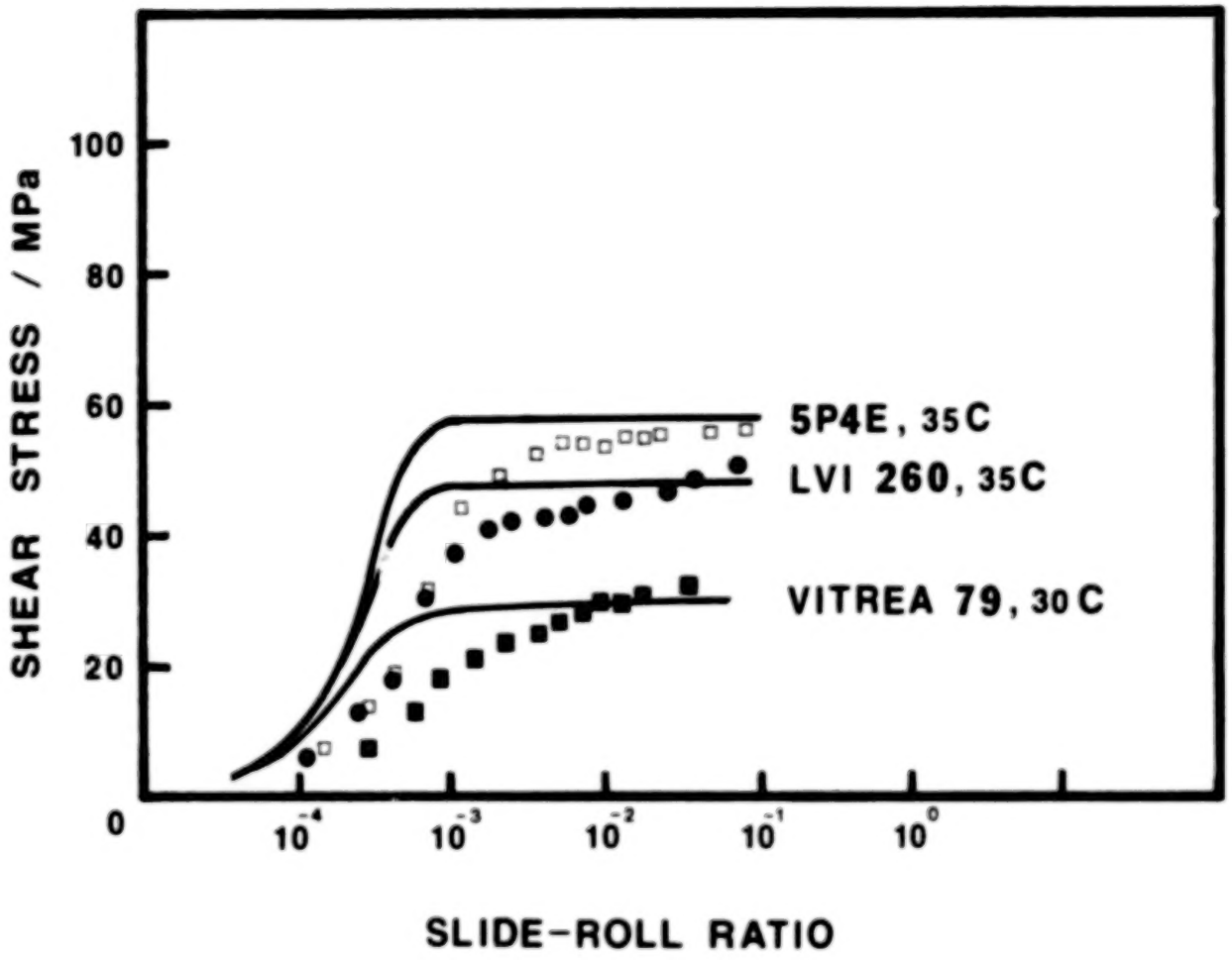

Figure 13. Traction Curves Predicted from Model and Experimental Data from Johnson and Tevaarwerk [8] for 5P4E, LVI 260, and VITREA 79 for Hertz Pressure of 1.0 GPa and rolling Speed of 0.22 m/s

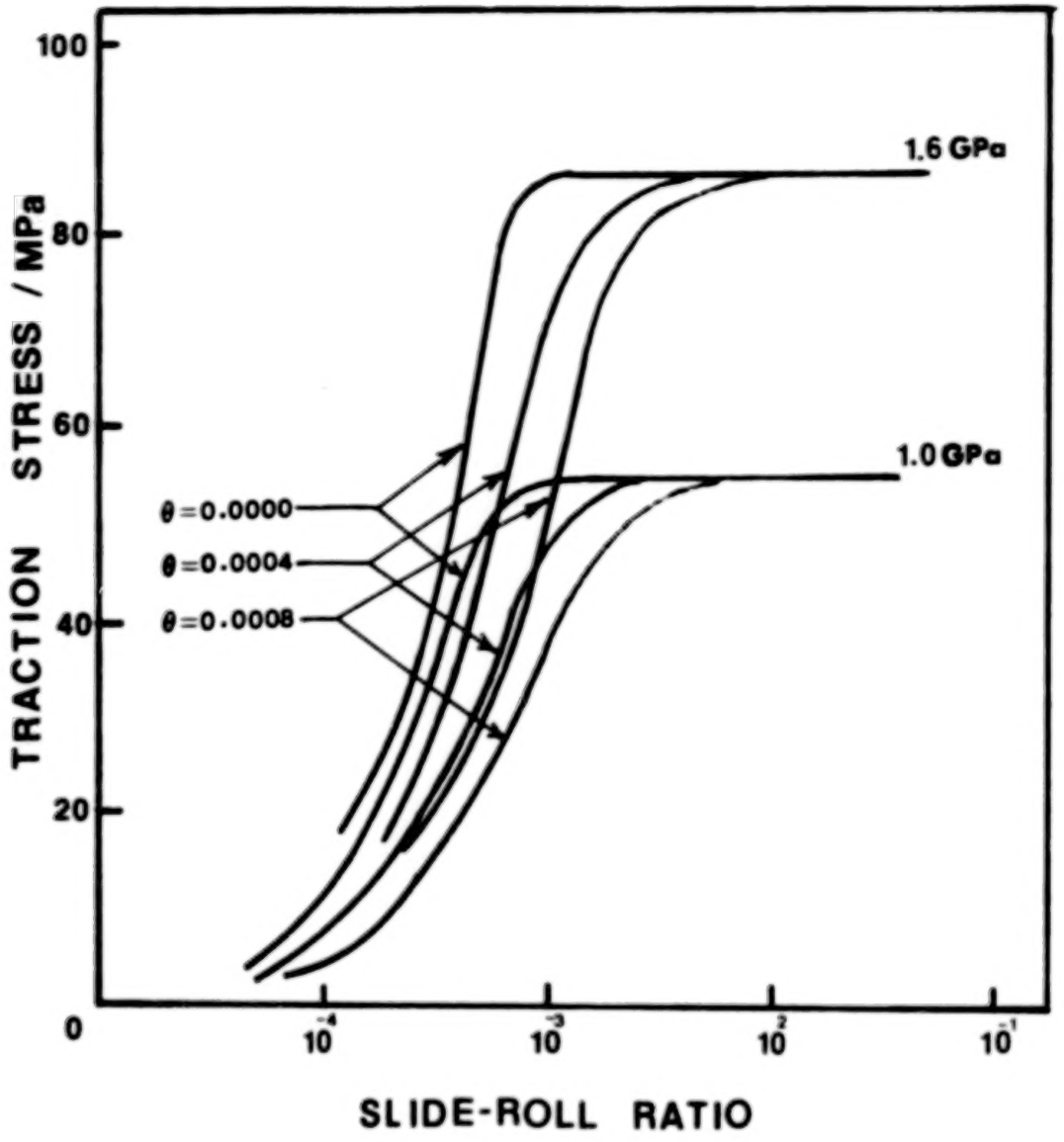

Figure 14. Traction Curves Predicted from Model for 5P4E at 45C, Rolling Speed of 0.22 m/s, and Hertz Pressures and Side-Slip Angle as Indicated.

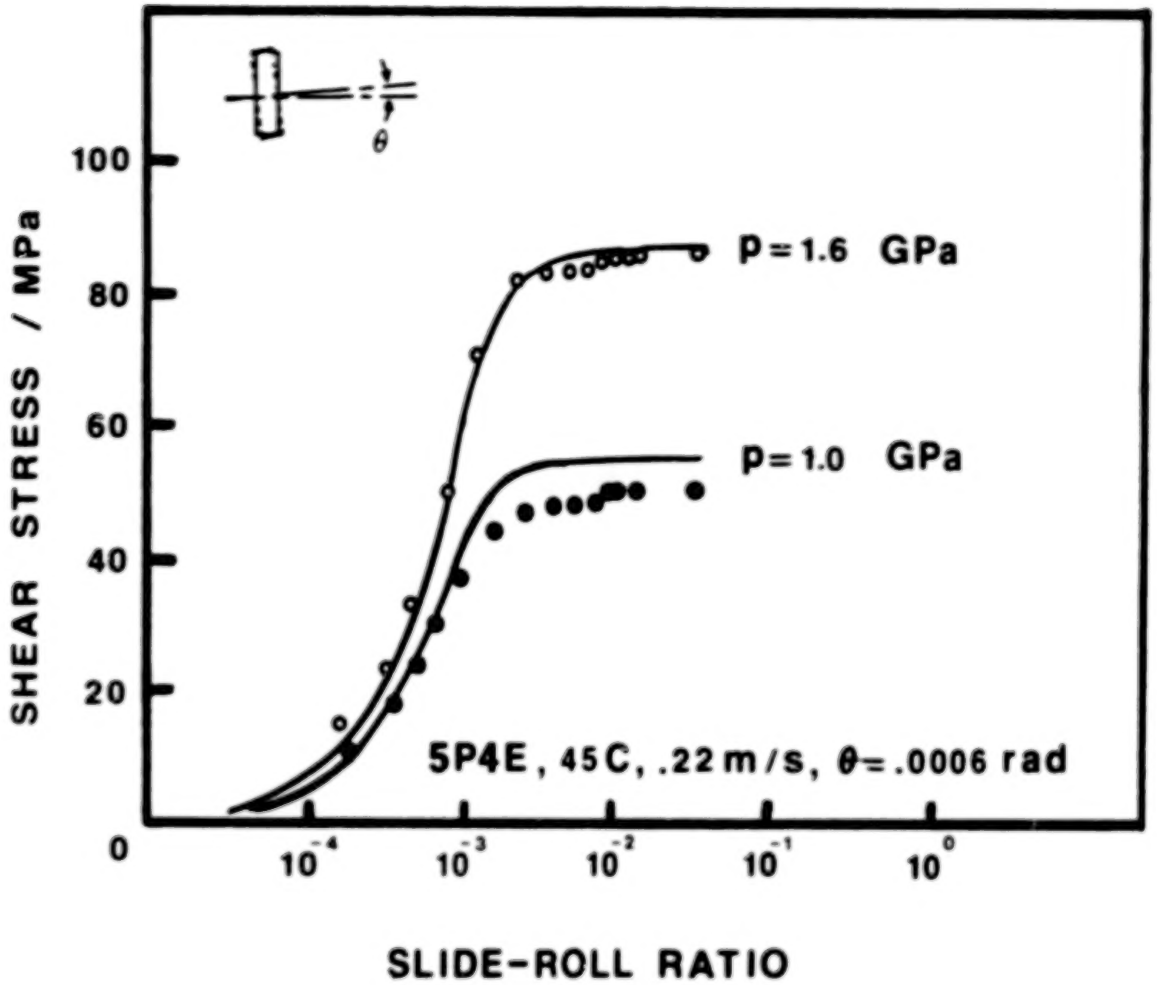

Figure 15. Traction Curves Predicted from Model for 5P4E at 45C, 0.22 m/s Rolling Speed, and 0.6 mradian Side-slip Compared with Measured Data from Johnson and Tevaarwerk [8] for indicated Hertz Pressure

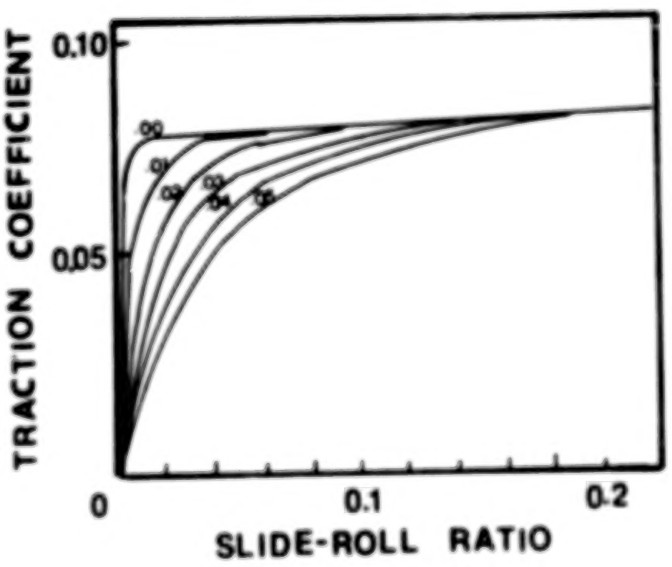

Figure 16. Traction Coefficient as Predicted from Model as a Function of Slide-Roll Ratio and Side-slip Angle in radians for N1 Mineral Oil at 30C, 1.0 m/s Rolling Speed, 0.86 GPa Hertz Pressure and Spin Radius of 36 mm.

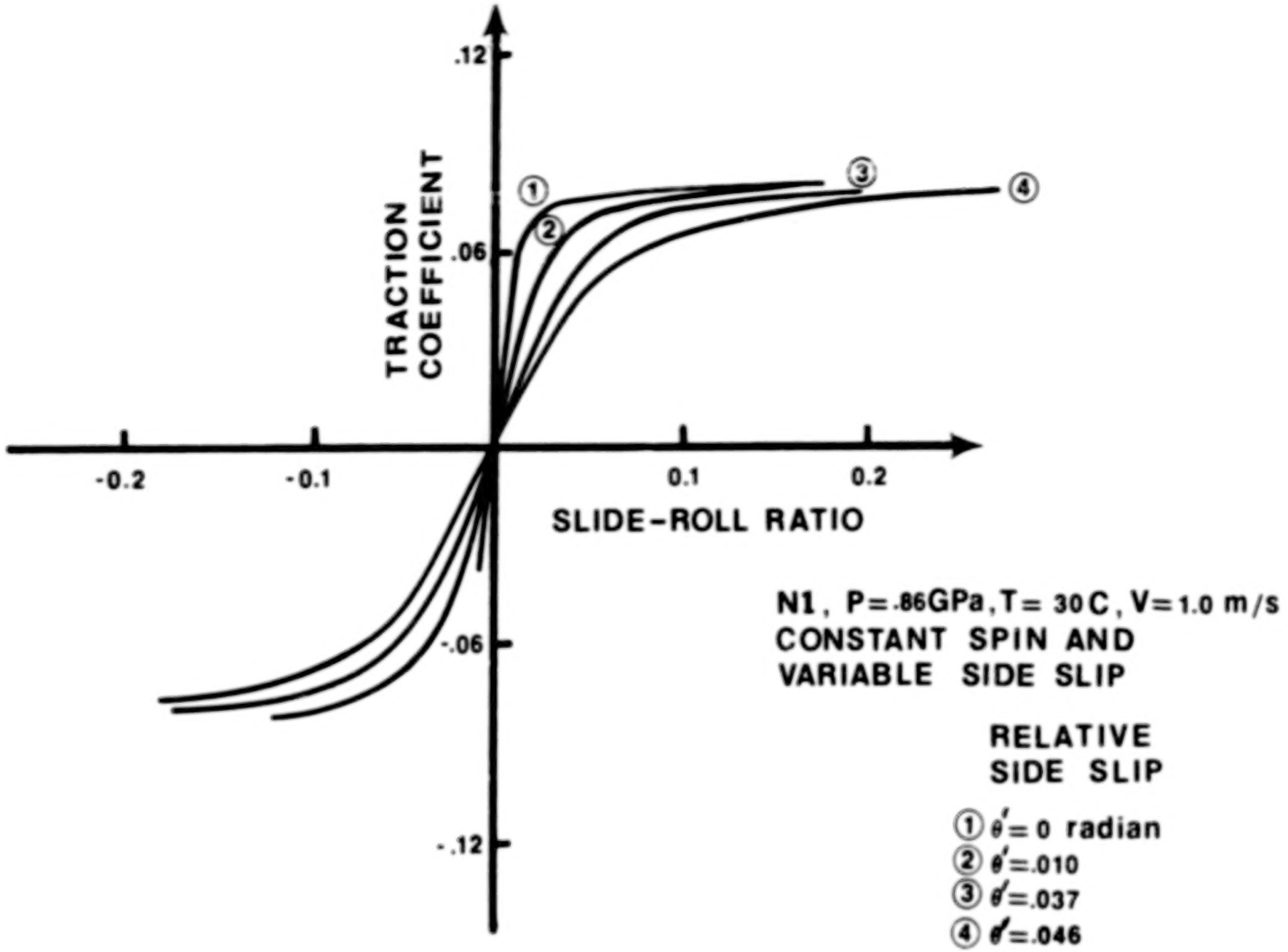

Figure 17. Measured Traction Coefficient versus Slide-roll Ratio for Various Relative Side-slip Angles, N1 Mineral Oil at 30C, 1.0 m/s Rolling Speed, 0.86 GPa Hertz Pressure and Constant Spin Radius of 36 mm

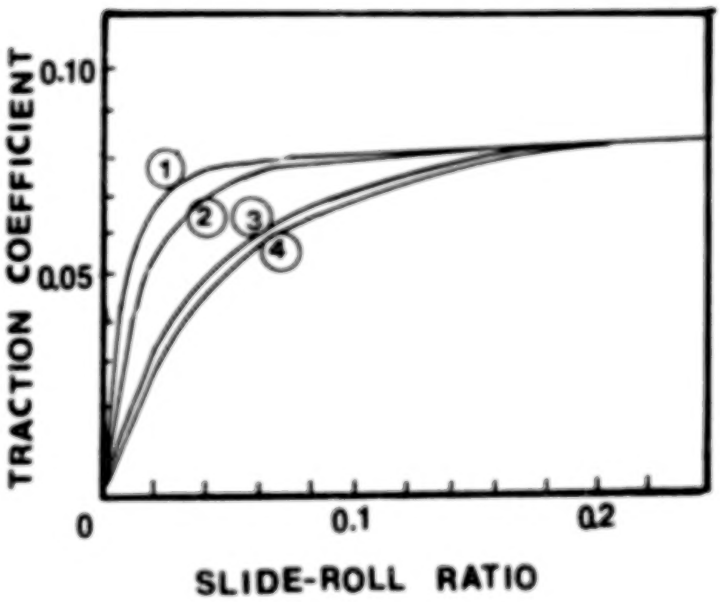

Figure 18. Predicted Traction Coefficient versus Slide-roll Ratio and Relative Side-slip, and Conditions

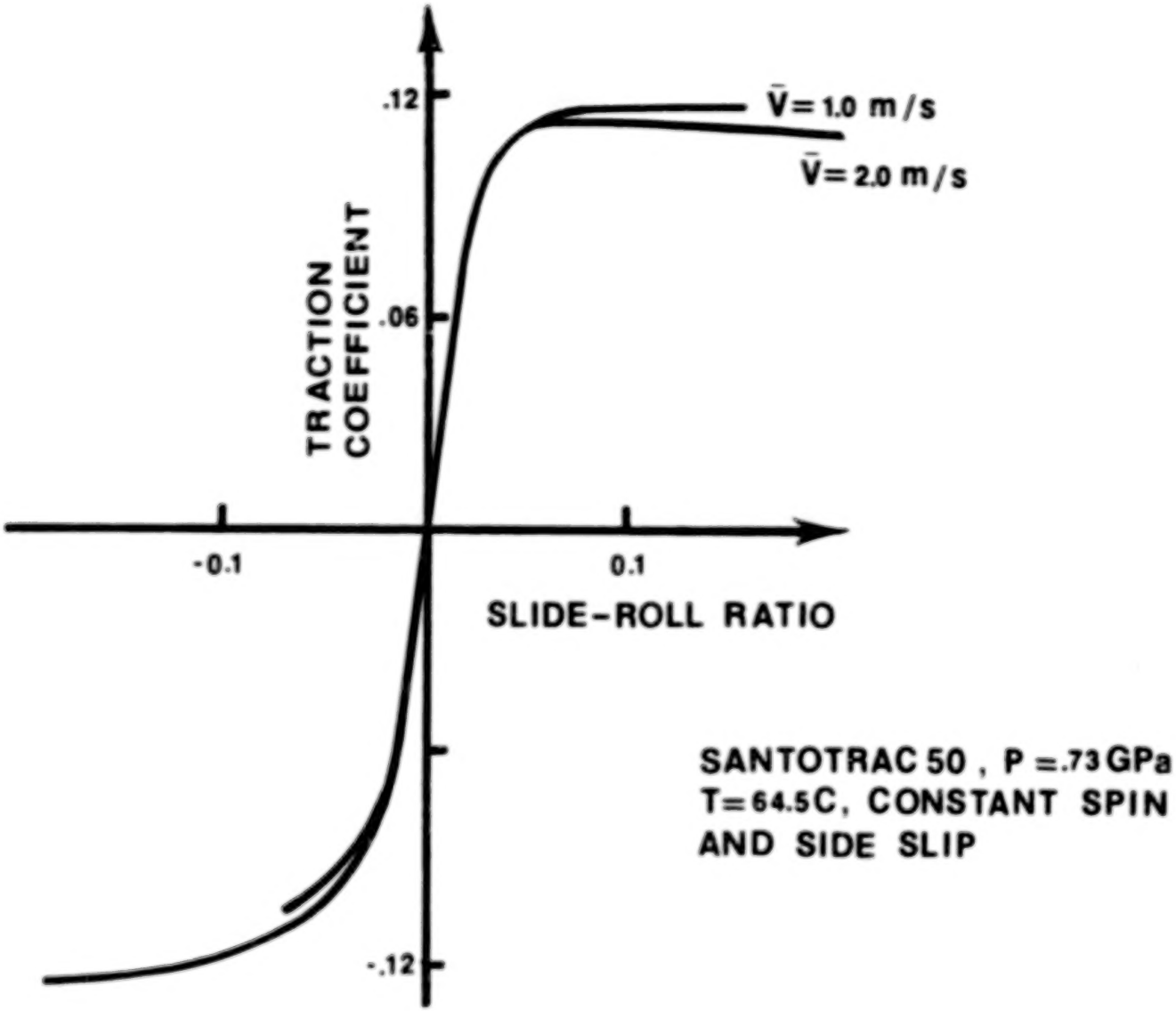

Figure 19. Measured Traction Conefficient versus Slide-roll Ratio for Santotrac 50 at 64.5C, Hertz Pressure 0.73 GPa with Constant Spin Radius and Side-slip, Rolling Velocity as Indicated

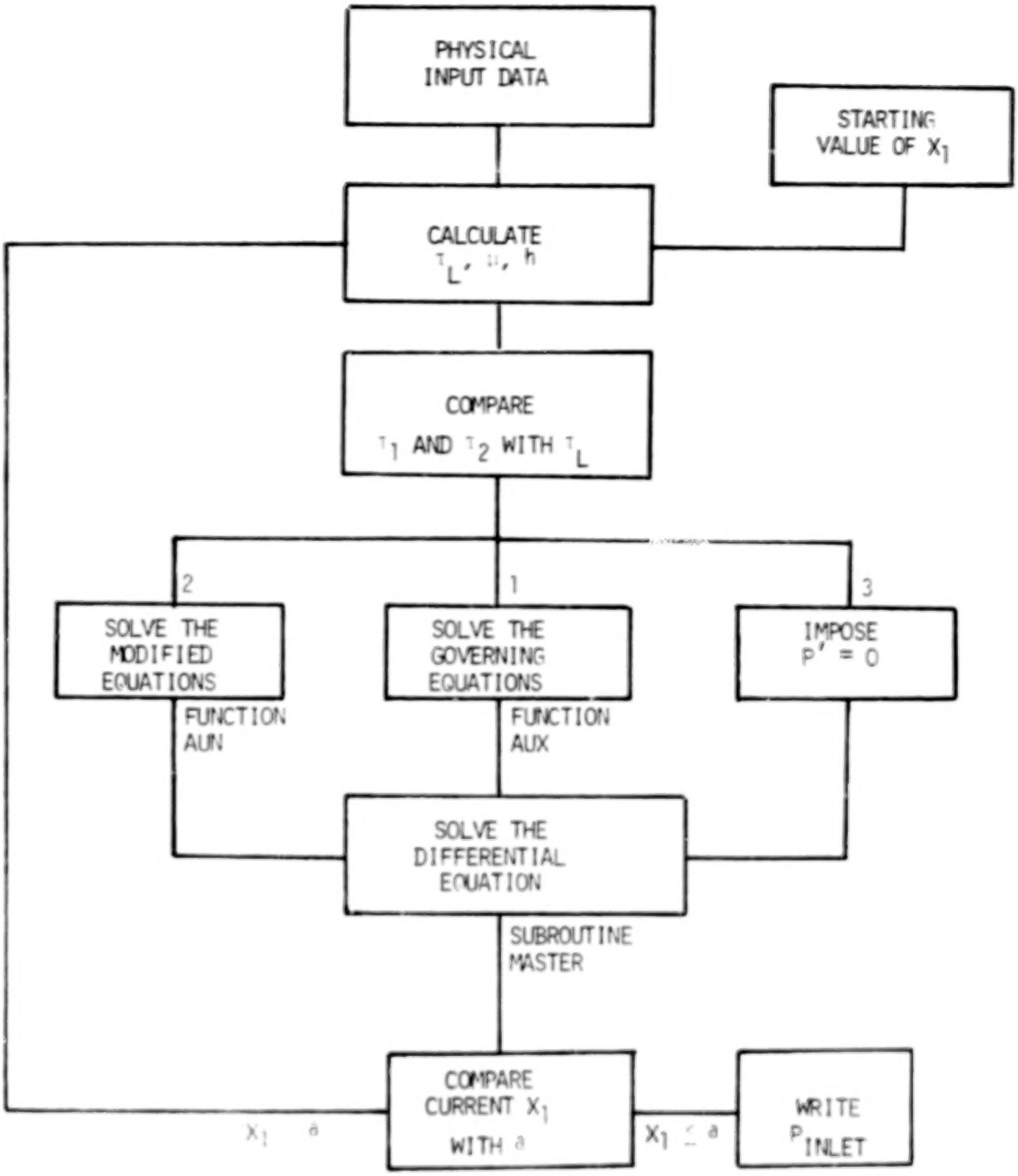

1. $\tau_1 < 0.9\,\tau_L$, $\tau_2 < 0.9\,\tau_L$
2. $\tau_1 < 0.9\,\tau_L$, $\tau_2 \geq 0.9\,\tau_L$
3. $\tau_1 > 0.9\,\tau_L$, $\tau_2 \geq 0.9\,\tau_L$

Figure 20. Solution scheme

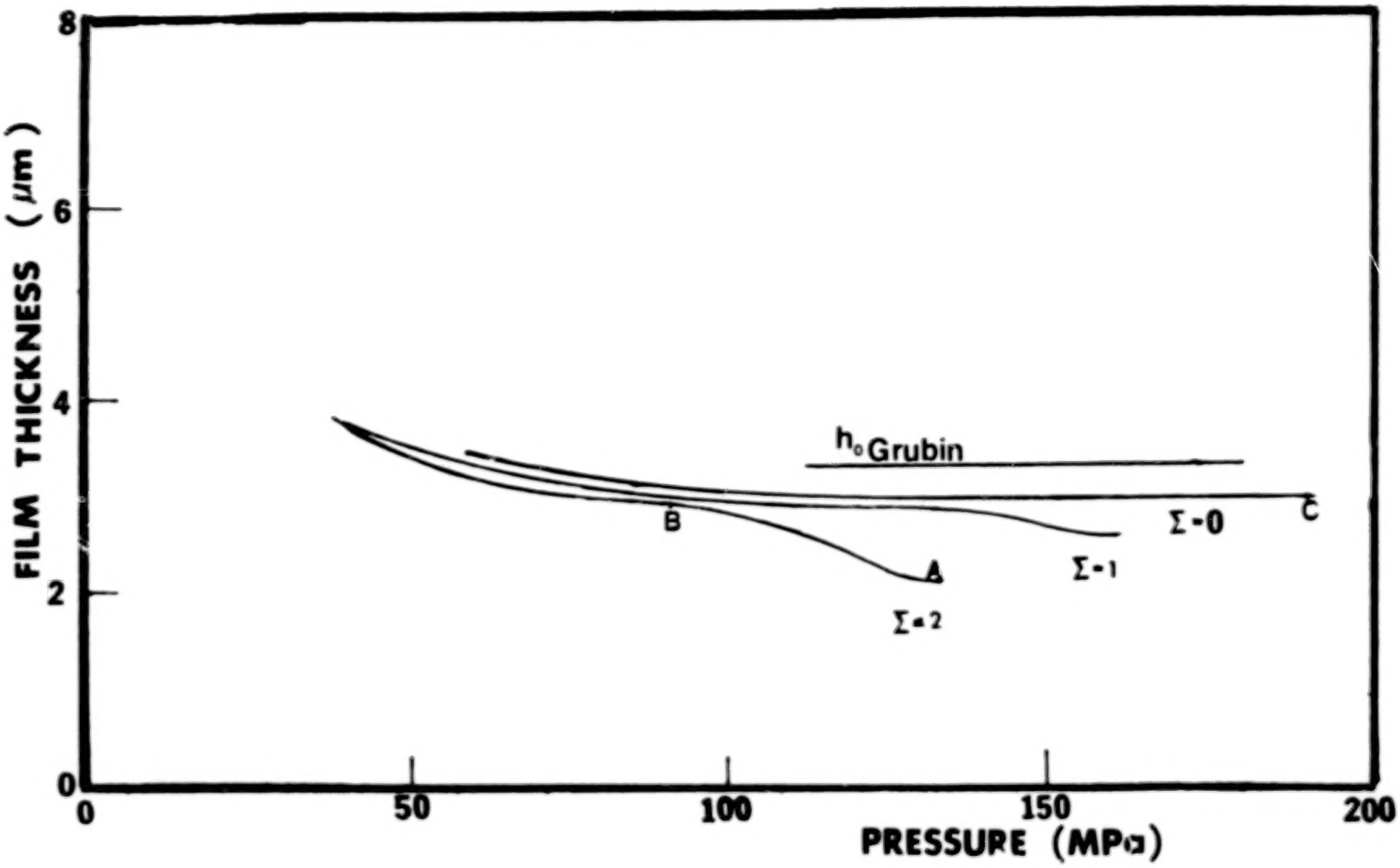

Figure 21. Film thickness versus inlet pressure, for different slide-roll ratios (w/L = 87.6 kN/m, p_H = 0.5 GPa, u = 2.54 m/s, μ_o = 410 mPas, τ_{L_o} = 0.69 MPa, m = 0.05).

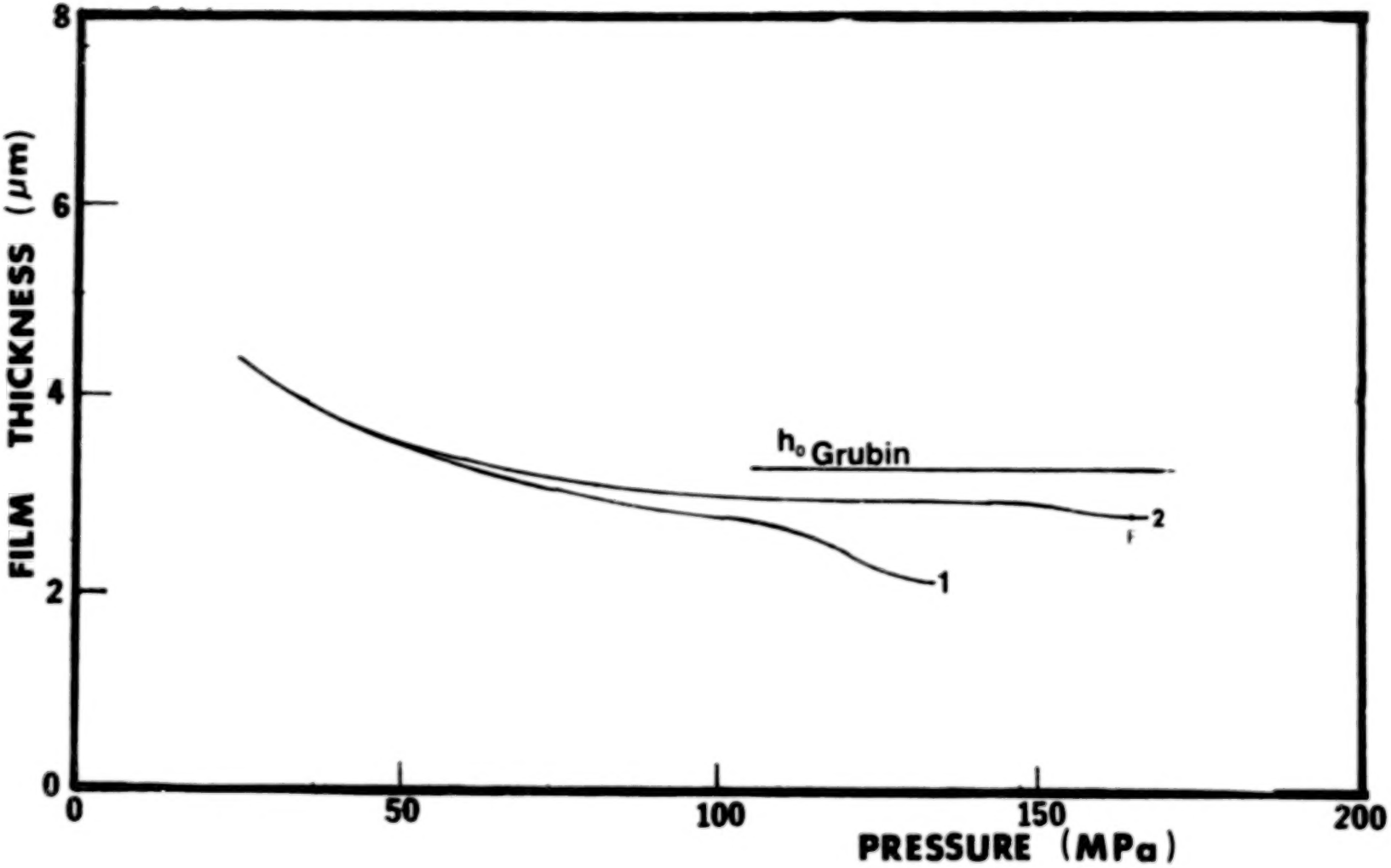

Figure 22. Film thickness versus inlet pressure, for different limiting shear stress parameters (w/L = 87.6 kN/m, p_H = 0.5 GPa, u = 2.54 m/s, μ_o = 410 mPas, Σ = 2).

1. τ_{L_o} = 0.69 MPa and m = 0.05
2. τ_{L_o} = 6.9 MPa and m = 0.1

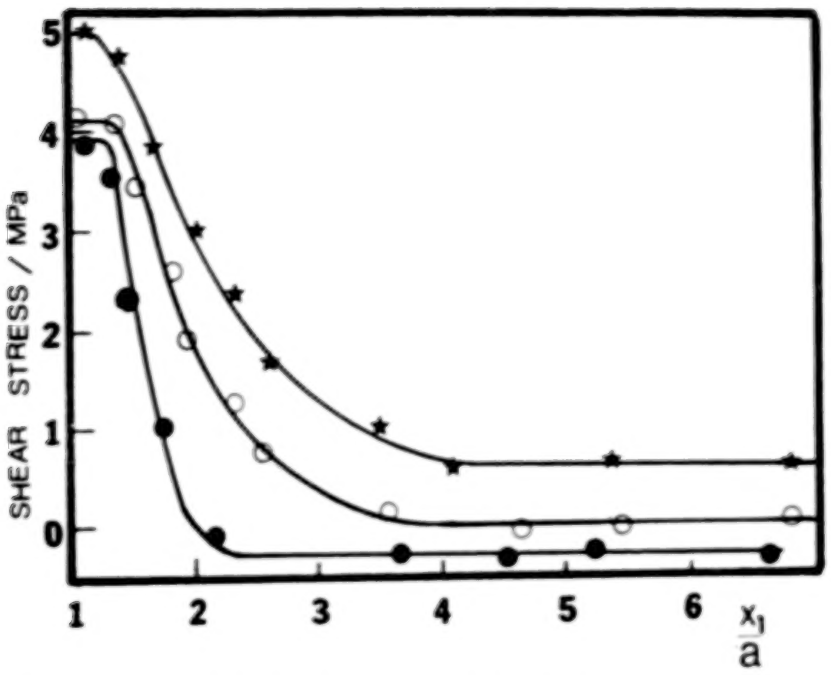

Figure 23. Shear stress distribution at the inlet zone for the conditions of point B of Figure 21

★: Limiting shear stress

O: Upper surface shear stress

●: Lower surface shear stress

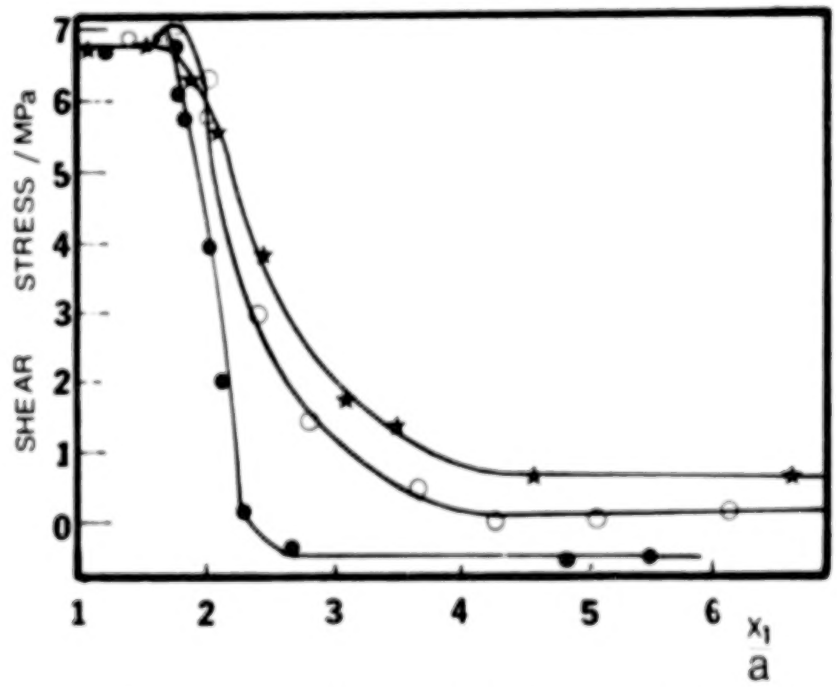

Figure 24. Shear stress distribution at the inlet zone for the conditions of point A of Figure 21 (Symbols as in Figure 23)

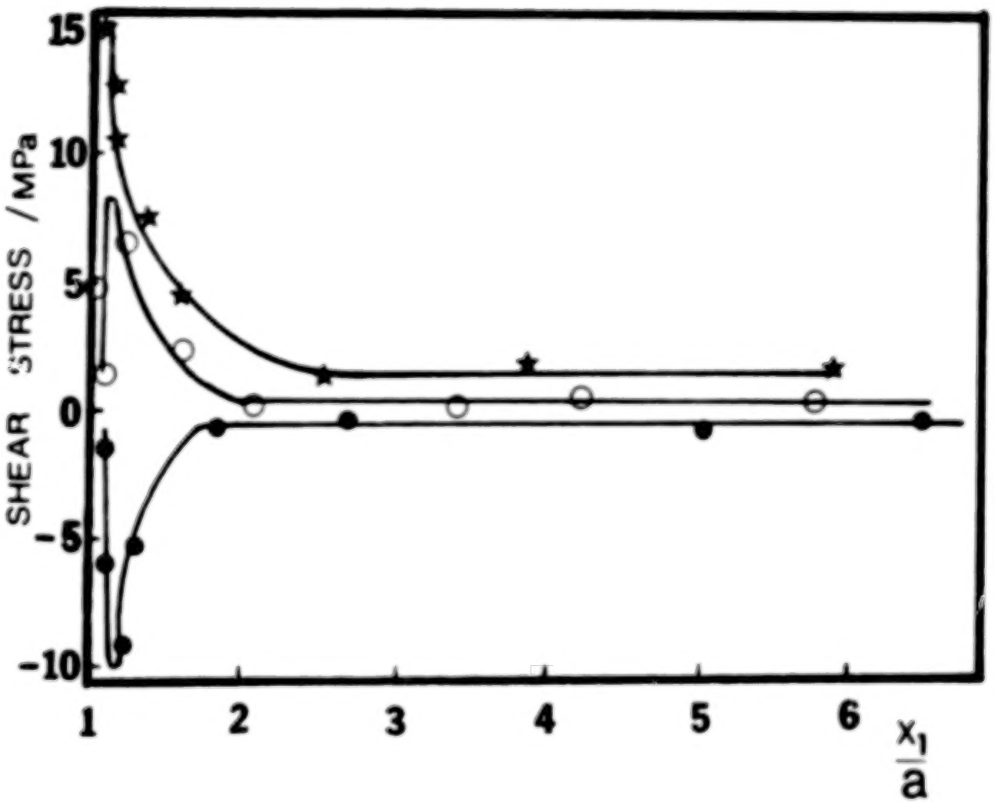

Figure 25. Shear stress distribution at the inlet zone for the conditions of point C of Figure 21 (Symbols as in Figure 23)

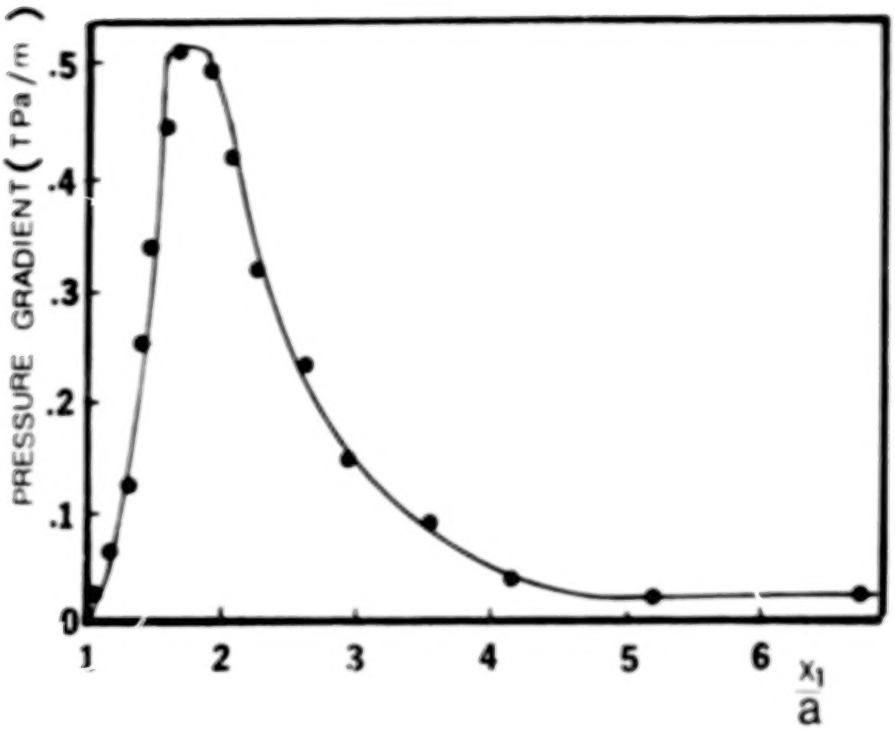

Figure 26. Pressure gradient distribution at the inlet zone for the conditions of point B of Figure 21

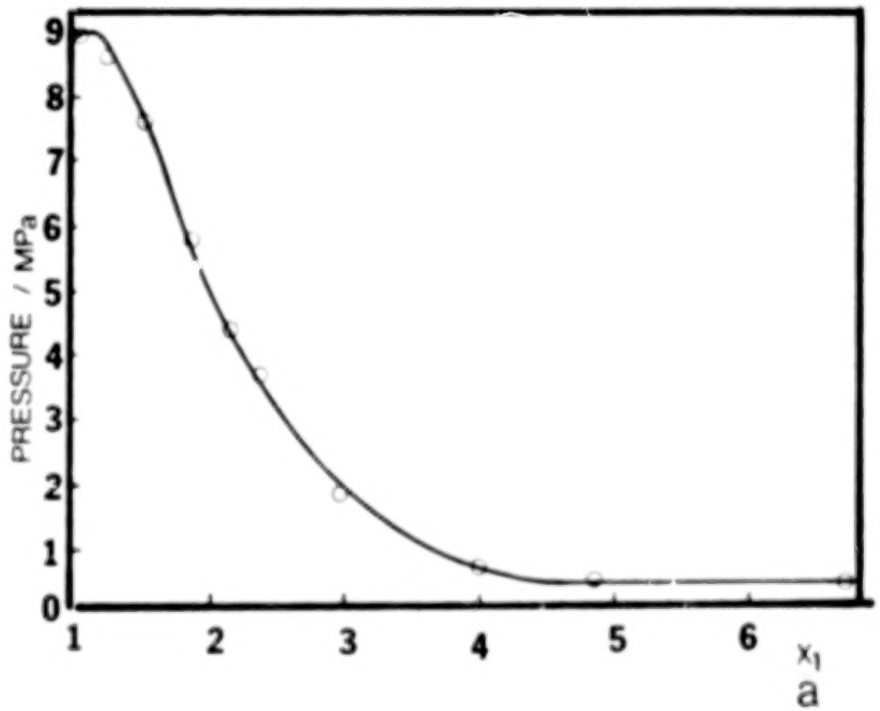

Figure 27. Pressure distribution at the inlet zone for the conditions of point B of Figure 21

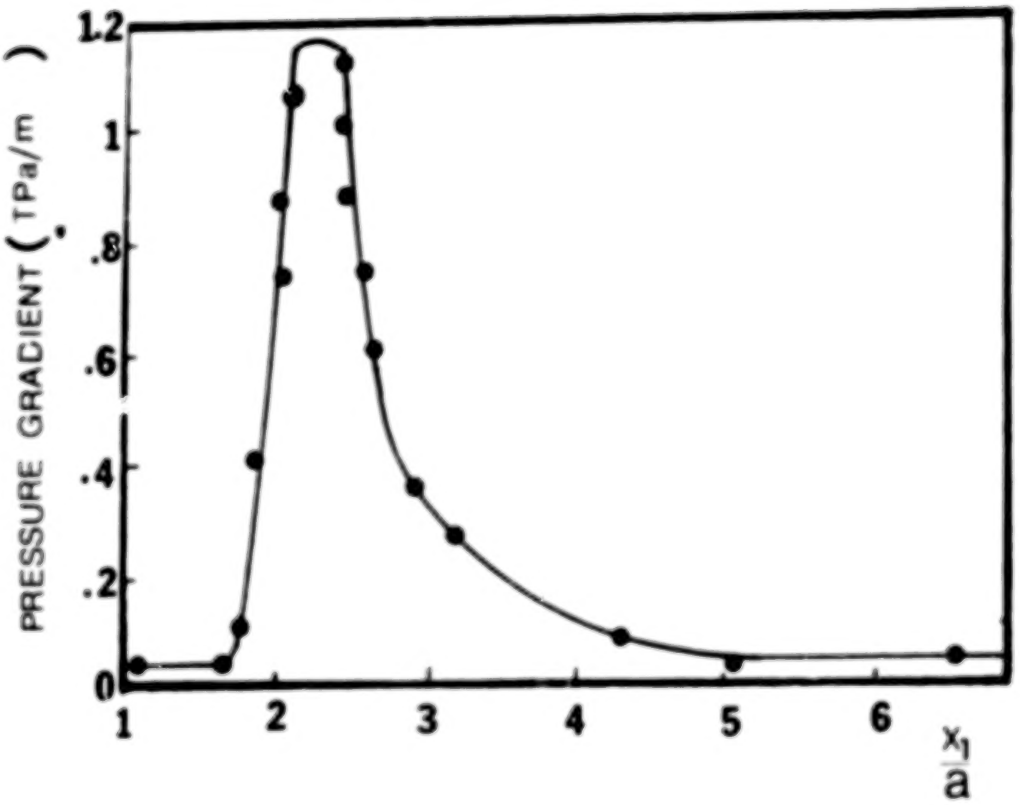

Figure 28. Pressure gradient distribution at the inlet zone for the conditions of point A of Figure 21

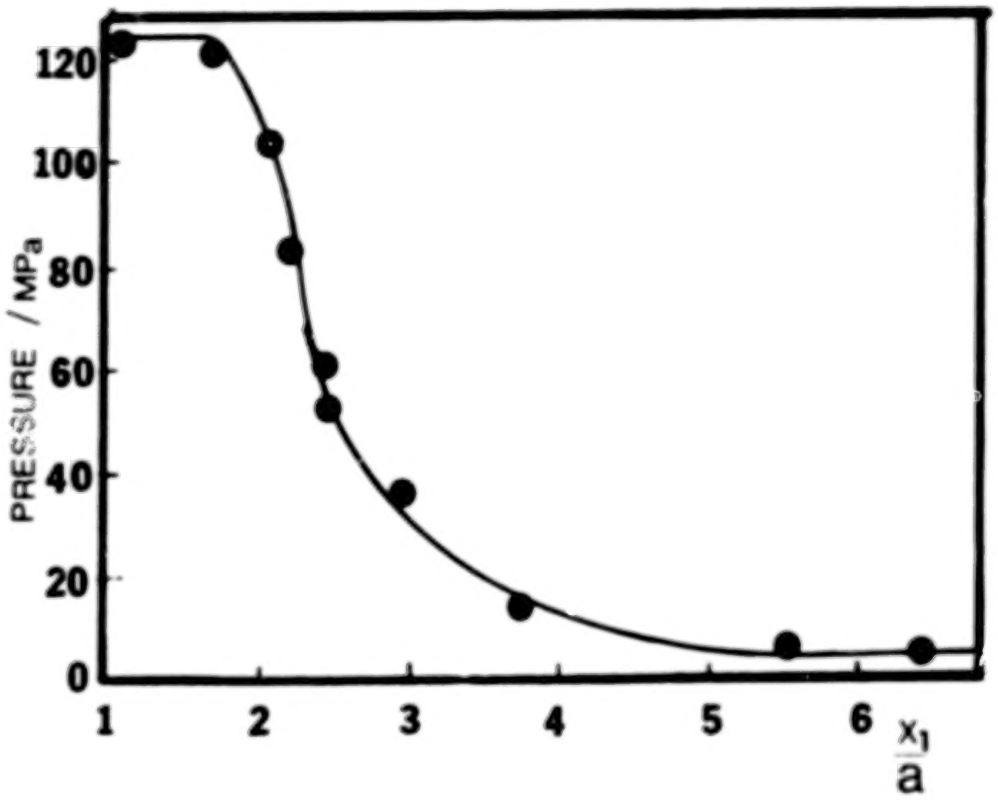

Figure 29. Pressure distribution at the inlet zone for the conditions of point A of Figure 2?

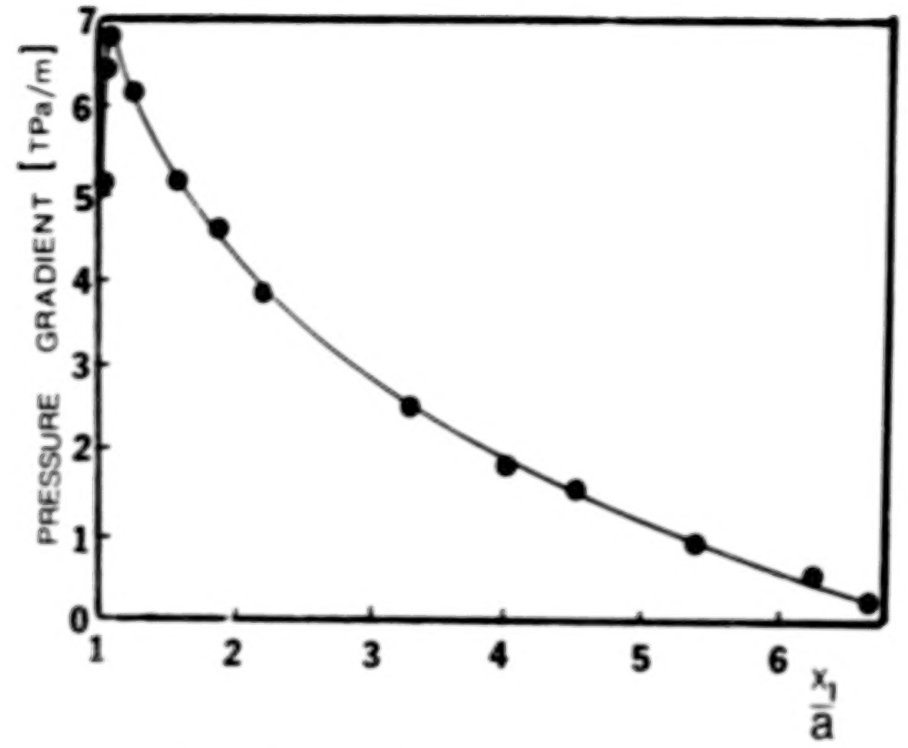

Figure 30. Pressure gradient distribution at the inlet zone for the conditions of point C of Figure 21

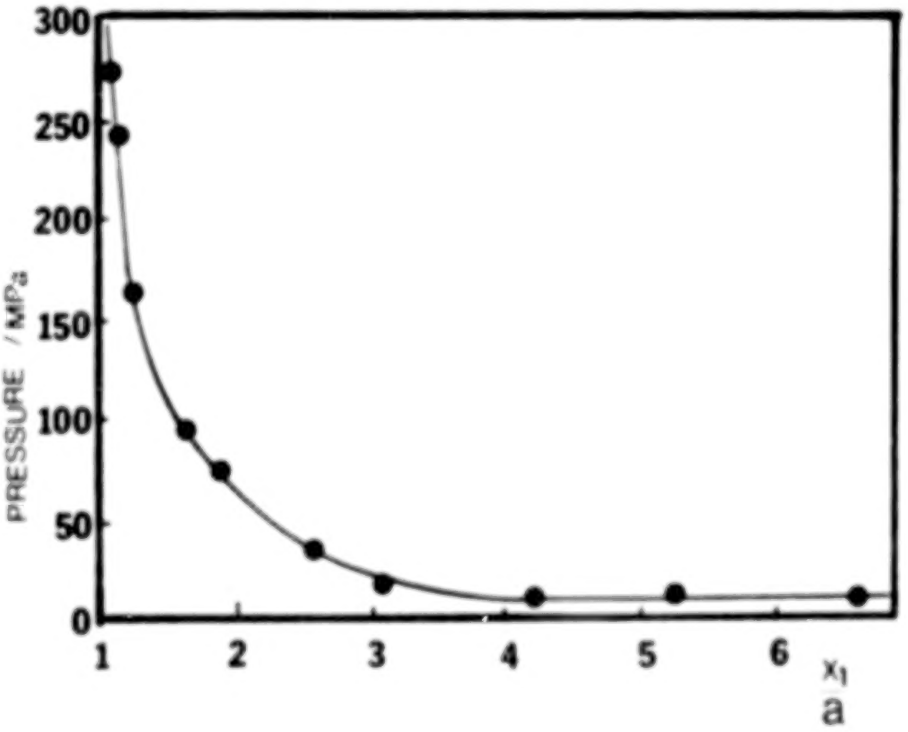

Figure 31. Pressure distribution at the inlet zone for the conditions of point C of Figure 21

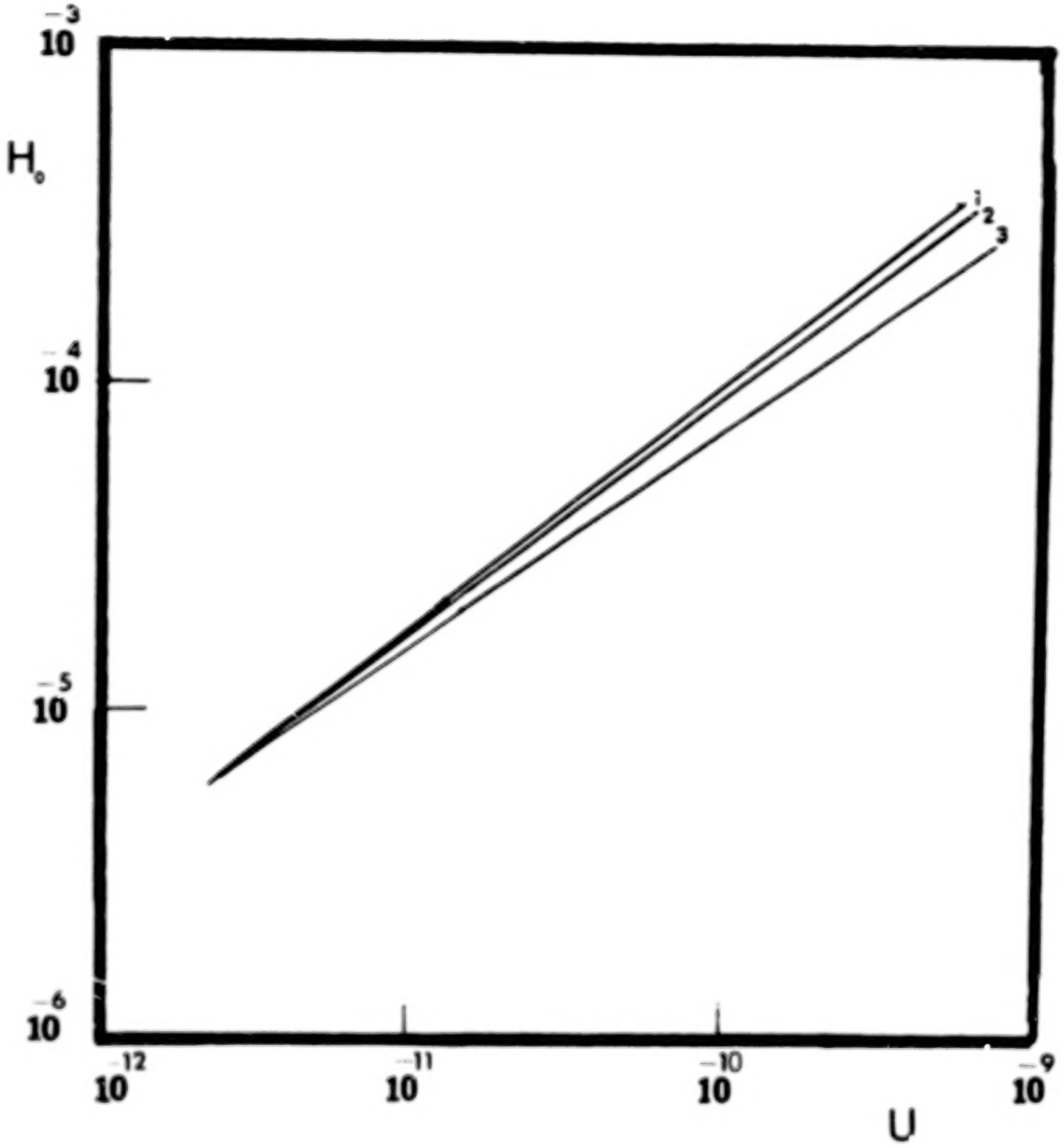

Figure 32. Dimensionless film thickness versus speed parameter, low load case

1. $H_{o_{Grubin}}$
2. $H_{o_{Model}}$ $\Sigma = 0$
3. $H_{o_{Model}}$ $\Sigma = 2$

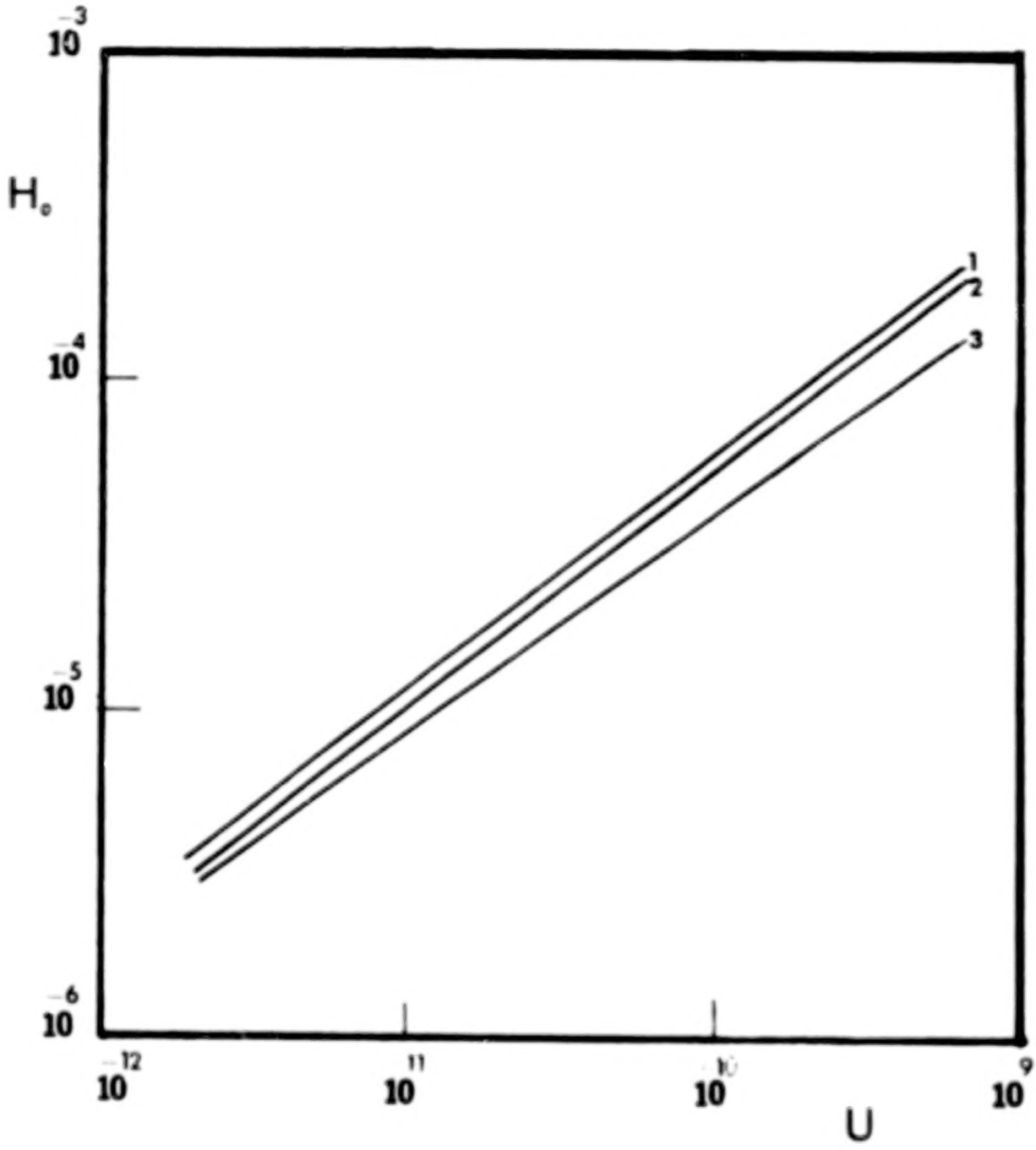

Figure 33. Dimensionless film thickness versus speed parameter, high load case (numbers as in Figure 32)

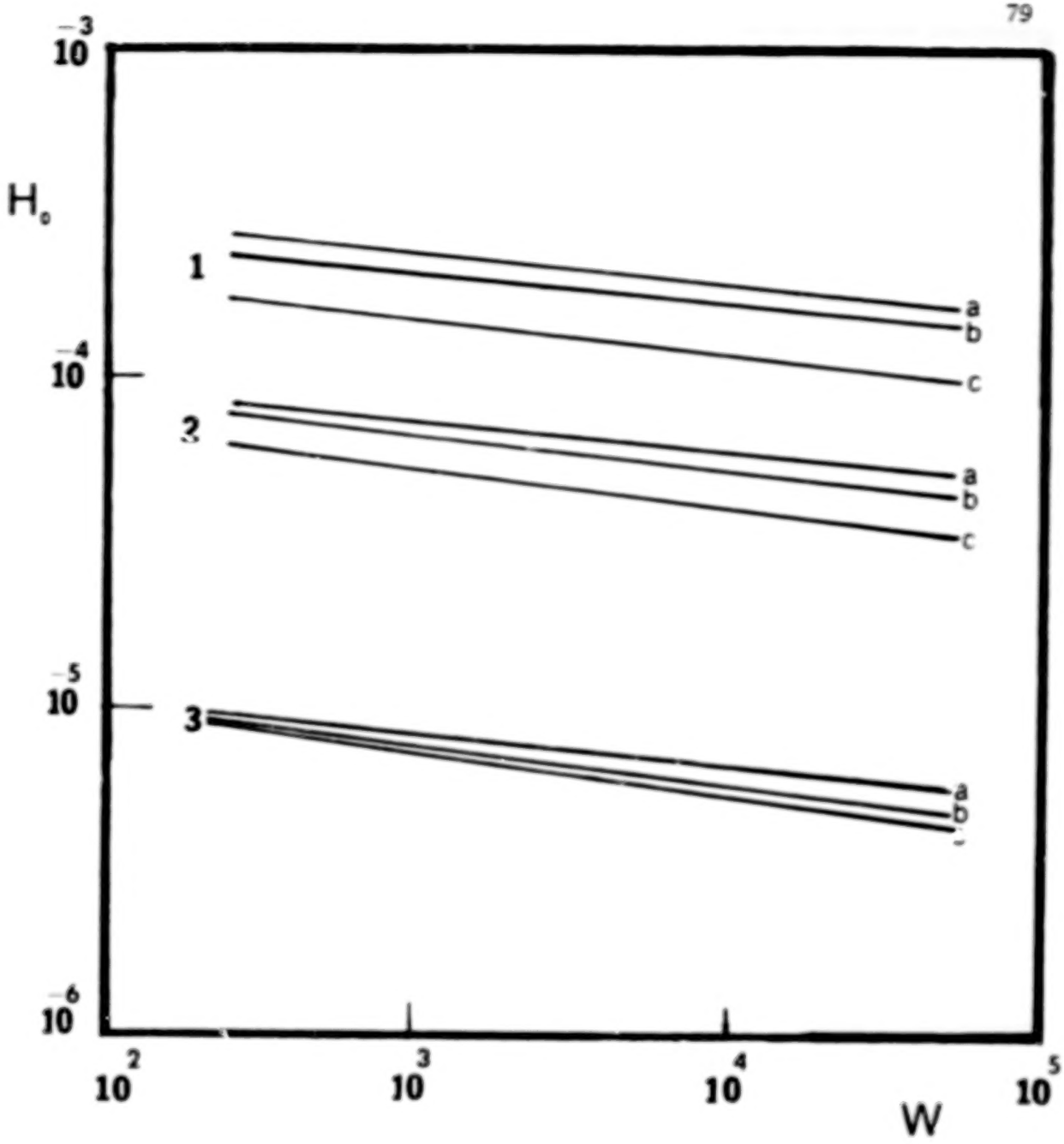

Figure 34. Dimensionless film thickness versus load parameter

1. $U = 3.96 \times 10^{-10}$ a. $H_{o_{Grubin}}$
2. $U = 7.92 \times 10^{-11}$ b. $H_{o_{Model}}$ $\Sigma = 0$
3. $U = 3.96 \times 10^{-12}$ c. $H_{o_{Model}}$ $\Sigma = 2$

TABLE OF CONTENTS

		Page	
NOMENCLATURE		v	1/A7
I.	INTRODUCTION	1	1/A9
II.	EXPERIMENTAL APPARATUS	5	1/A13
	A. Low Pressure Stress-Strain Apparatus: 0.7 GPa B. Constant Pressure Stress-Strain Apparatus 1.1 GPa		
III.	EXPERIMENTAL LUBRICANTS	9	1/B3
IV.	EXPERIMENTAL RESULTS	10	1/B4
	A. Liquid Lubricants B. Solid Polymers		
V.	APPLICATION OF THE MODEL TO EHD TRACTION PREDICTIONS	14	1/B8
VI.	APPLICATION OF THE MODEL TO EHD FILM THICKNESS PREDICTION	18	1/B12
	A. Shear Rheological Model B. Derivation of the Governing Equations C. Method of Solution D. Physical Input Data E. Results F. Discussion G. Conclusions		
REFERENCES		41	1/D7
APPENDICES			
A.	DESCRIPTION OF EXPERIMENTAL FLUIDS	43	1/D9
B.	DERIVATION OF PRESSURE GRADIENT EQUATIONS	47	1/D13

1. Report No.	2. Government Accession No.	3. Recipient's Catalog No.
NASA CR-3272		

4. Title and Subtitle	5. Report Date
SURFACE TEMPERATURES AND GLASSY STATE INVESTIGATIONS IN TRIBOLOGY - PART III	April 1980
	6. Performing Organization Code
7. Author(s)	8. Performing Organization Report No.
Scott S. Bair and Ward O. Winer	None
	10. Work Unit No.
9. Performing Organization Name and Address	11. Contract or Grant No.
Georgia Institute of Technology Atlanta, Georgia 30332	NSG-3106
	13. Type of Report and Period Covered
12. Sponsoring Agency Name and Address	Contractor Report
National Aeronautics and Space Administration Washington, D.C. 20546	14. Sponsoring Agency Code

15. Supplementary Notes

Final report. Project Manager, William R. Jones, Jr., Fluid System Components Division, NASA Lewis Research Center, Cleveland, Ohio 44135.

16. Abstract

The research reported covers the continued development of the limiting shear stress shear rheological model. This development consists of both property measurements pursuant to the use of the constitutive equation and the application of the constitutive equation to EHD traction and film thickness predictions. It has been shown that the history the material undergoes influences the limiting shear stress. Previously materials were subjected to isobaric cooling. Techniques were developed to subject materials to isothermal compression which is similar to what occurs in EHD contacts. The limiting shear stress from the isothermal compression is approximately 10 percent less than that from isobaric cooling. This more relevant determination of limiting shear stress and elastic shear modulus is reported for several lubricants. In addition, an apparatus has also been developed for measuring the shear stress-strain behavior of solid lubricating materials. Four materials have been examined under pressure. They exhibit elastic and limiting shear stress behavior similar to that of liquid lubricants. The application of the limiting shear stress model to traction predictions has been extended employing the primary material properties. These predictions indicate that the isothermal compression limiting shear stress correlates with and predicts very well the maximum traction for a given lubricant. Small amounts of side slip and twist have been incorporated in the model and are shown to have great influence on the rising portion of the traction curve at low slide-roll ratio. It is shown that small misalignments causing side slip of the order of half a milliradian will result in the traction curve predicted by the model to coincide extremely well with experimental data even in the rising portion of the traction curve at low slide-roll ratios. These predictions have been compared both with work from other laboratories and traction curve measurements made in this laboratory and reported here. The shear rheological model has also been applied to a Grubin-like EHD inlet analysis for predicting film thicknesses when employing the limiting shear stress model material behavior.

17. Key Words (Suggested by Author(s))	18. Distribution Statement
Liquid lubricants Elastohydrodynamic lubrication Glass transition	Unclassified - unlimited Subject Category 27

19. Security Classif. (of this report)	20. Security Classif. (of this page)	21. No. of Pages	22. Price*
Unclassified	Unclassified	83	A05

* For sale by the National Technical Information Service, Springfield, Virginia 22161

NASA-Langley, 1980

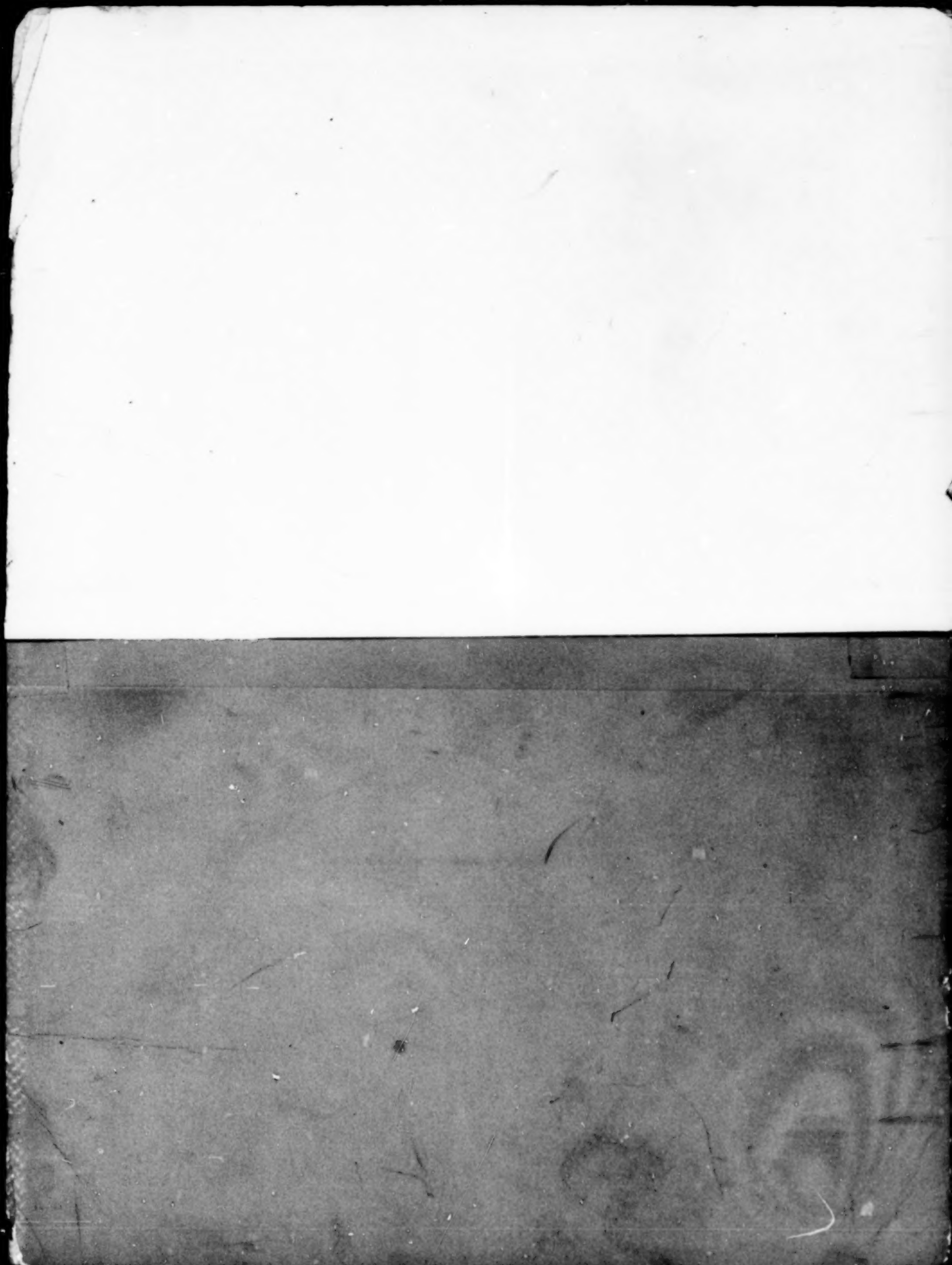

END

June 30, 1981